NRC FORM 464 Part I (01-2018)

U.S. NUCLEAR REGULATORY COMMISSION

RESPONSE TO FREEDOM OF INFORMATION ACT (FOIA) REQUEST

FOIA	RESPONSE NUMBER
NRC-2018-000182	2

RESPONSE TYPE ☐ INTERIM ☑ FINAL

REQUESTER:	DATE:
Julian Tarver	01/12/2018

DESCRIPTION OF REQUESTED RECORDS:

ML100740454, ML101470489, and ML100540294

PART I. -- INFORMATION RELEASED

You have the right to seek assistance from the NRC's FOIA Public Liaison. Contact information for the NRC's FOIA Public Liaison is available at https://www.nrc.gov/reading-rm/foia/contact-foia.html

- ☑ Agency records subject to the request are already available on the Public NRC Website, in Public ADAMS or on microfiche in the NRC Public Document Room.
- ☑ Agency records subject to the request are enclosed.
- ☐ Records subject to the request that contain information originated by or of interest to another Federal agency have been referred to that agency (see comments section) for a disclosure determination and direct response to you.
- ☐ We are continuing to process your request.
- ☑ See Comments.

PART I.A -- FEES

AMOUNT*

*See Comments for details

- ☐ You will be billed by NRC for the amount listed.
- ☐ You will receive a refund for the amount listed.
- ☐ Fees waived.

NO FEES

- ☑ Minimum fee threshold not met.
- ☐ Due to our delayed response, you will not be charged fees.

PART I.B -- INFORMATION NOT LOCATED OR WITHHELD FROM DISCLOSURE

- ☐ We did not locate any agency records responsive to your request. *Note*: Agencies may treat three discrete categories of law enforcement and national security records as not subject to the FOIA ("exclusions"). 5 U.S.C. 552(c). This is a standard notification given to all requesters; it should not be taken to mean that any excluded records do, or do not, exist.
- ☑ We have withheld certain information pursuant to the FOIA exemptions described, and for the reasons stated, in Part II.
- ☐ Because this is an interim response to your request, you may not appeal at this time. We will notify you of your right to appeal any of the responses we have issued in response to your request when we issue our final determination.
- ☑ You may appeal this final determination within 90 calendar days of the date of this response by sending a letter or e-mail to the FOIA Officer, at U.S. Nuclear Regulatory Commission, Washington, D.C. 20555-0001, or FOIA.Resource@nrc.gov. Please be sure to include on your letter or email that it is a "FOIA Appeal." You have the right to seek dispute resolution services from the NRC's Public Liaison, or the Office of Government Information Services (OGIS). Contact information for OGIS is available at https://ogis.archives.gov/about-ogis/contact-information.htm

PART I.C COMMENTS (Use attached Comments continuation page if required)

In interim response #1 (dated 12/21/2017), we provided you copies of ML101470489 and ML100540294, which were already publicly available in their entirety. In this final response, we are providing you with a redacted copy of ML100740454 (which is also already publicly available as ML101650422). The redacted portions have been determined to be exempt from disclosure under FOIA exemption 7(F) (See Form 464-Part 2).

Signature - Freedom of Information Act Officer or Designee

James Chilcoat for SRM 1/12/18

NRC FORM 464 Part II
(03-2017)

U.S. NUCLEAR REGULATORY COMMISSION

RESPONSE TO FREEDOM OF INFORMATION ACT (FOIA) REQUEST

FOIA: NRC-2018-000182#2

DATE: 01/12/2018

PART II.A -- APPLICABLE EXEMPTIONS

Records subject to the request are being withheld in their entirety or in part under the FOIA exemption(s) as indicated below (5 U.S.C. 552(b)).

- ☐ Exemption 1: The withheld information is properly classified pursuant to an Executive Order protecting national security information.
- ☐ Exemption 2: The withheld information relates solely to the internal personnel rules and practices of NRC.
- ☐ Exemption 3: The withheld information is specifically exempted from public disclosure by the statute indicated.
  - ☐ Sections 141-145 of the Atomic Energy Act, which prohibits the disclosure of Restricted Data or Formerly Restricted Data (42 U.S.C. 2161-2165).
  - ☐ Section 147 of the Atomic Energy Act, which prohibits the disclosure of Unclassified Safeguards Information (42 U.S.C. 2167).
  - ☐ 41 U.S.C. 4702(b), which prohibits the disclosure of contractor proposals, except when incorporated into the contract between the agency and the submitter of the proposal.
- ☐ Exemption 4: The withheld information is a trade secret or confidential commercial or financial information that is being withheld for the reason(s) indicated.
  - ☐ The information is considered to be proprietary because it concerns a licensee's or applicant's physical protection or material control and accounting program for special nuclear material pursuant to 10 CFR 2.390(d)(1).
  - ☐ The information is considered to be another type or confidential business (proprietary) information.
  - ☐ The information was submitted by a foreign source and received in confidence pursuant to 10 CFR 2.390(d)(2).
- ☐ Exemption 5: The withheld information consists of interagency or intraagency records that are normally privileged in civil litigation.
  - ☐ Deliberative process privilege.
  - ☐ Attorney work product privilege.
  - ☐ Attorney-client privilege.
- ☐ Exemption 6: The withheld information from a personnel, medical, or similar file, is exempted from public disclosure because its disclosure would result in a clearly unwarranted invasion of personal privacy.
- ☑ Exemption 7: The withheld information consists of records compiled for law enforcement purposes and is being withheld for the reason(s) indicated.
  - ☐ (A) Disclosure could reasonably be expected to interfere with an open enforcement proceeding.
  - ☐ (C) Disclosure could reasonably be expected to constitute an unwarranted invasion of personal privacy.
  - ☐ (D) The information consists of names and other information the disclosure of which could reasonably be expected to reveal identities of confidential sources.
  - ☐ (E) Disclosure would reveal techniques and procedures for law enforcement investigations or prosecutions, or guidelines that could reasonably be expected to risk circumvention of the law.
  - ☑ (F) Disclosure could reasonably be expected to endanger the life or physical safety of an individual.
  - ☐ Other

PART II.B -- DENYING OFFICIALS

In accordance with 10 CFR 9.25(g) and 9.25(h) of the U.S. Nuclear Regulatory Commission regulations, the official(s) listed below have made the determination to withhold certain information responsive to your request.

DENYING OFFICIAL	TITLE/OFFICE	RECORDS DENIED	APPELLATE OFFICIAL	
			EDO	SECY
Stephanie A. Blaney	FOIA Officer	security-sensitive information	☑	☐
			☐	☐
			☐	☐

Appeals must be made in writing within 90 calendar days of the date of this response by sending a letter or email to the FOIA Officer, at U.S. Nuclear Regulatory Commission, Washington, D.C. 20555-0001, or FOIA.Resource@nrc.gov. Please be sure to include on your letter or email that it is a "FOIA Appeal."

10CFR 50.30

ARMED FORCES RADIOBIOLOGY RESEARCH INSTITUTE
8901 WISCONSIN AVENUE
BETHESDA, MARYLAND 20889-5603

March 4, 2010

U.S. Nuclear Regulatory Commission
ATTN: Document Control Desk
Washington, DC 20555-0001

Sir:

On June 24, 2004, the Armed Forces Radiobiology Research Institute submitted an application to renew the operating license for its research reactor (License R-84, Docket 50-170). The enclosed two revised Safety Analysis Report chapters replace the indicated sections in the 2004 submittal:

1. New Chapter 4 replaces original Sections 4.1-4.10 and 4.16
2. New Chapter 13 replaces original Section 3.4.1 and Chapter 6

Further revised Safety Analysis Report chapters will be submitted as soon as possible.

The point of contact concerning this submittal is Mr. Stephen Miller, 301-295-9245.

I declare under penalty of perjury that the statements above and all enclosed documents are true and correct.

STEPHEN I. MILLER
Reactor Facility Director

Encl:
as

A053
NRR

4 REACTOR DESCRIPTIONS

4.1 SUMMARY DESCRIPTION

The AFRRI-TRIGA Mark-F reactor was designed and manufactured by General Atomics and installed at AFRRI in 1962. The reactor is a tank-type light water reactor, with a horizontally movable core. The reactor tank is embedded in ordinary concrete. The cylindrical core consists of up to 87 standard TRIGA stainless steel-clad, cylindrical fuel elements with U-$ZrH_{1.7}$ as the fuel matrix material enriched to less than 20 percent in U^{235}, four aluminum or stainless steel-clad borated graphite control rods with air, fuel, aluminum, or poison (neutron absorber) follower and a startup neutron source and guide tube. The core moderator consists of both water and the zirconium hydride in the fuel. The reactor core is reflected on the top and bottom by graphite end plugs in each fuel element, and at the periphery by water. The cylindrical fuel elements and the control rods are positioned in the core in five concentric rings surrounding the centrally located transient control rod. The fuel elements and control rod guide tubes are held in place with top and bottom grid plates. The grid plates are attached to a cylindrical shroud which surrounds the core.

There are three principal and one optional experimental facilities associated with the AFRRI-TRIGA reactor. These are Exposure Room #1, Exposure Room #2, removable in-core experiment tube(s) (CET), and the Pneumatic Transfer System (installed as required). Experiments can also be placed either in the reactor tank or in the reactor core between the fuel elements.

The AFRRI-TRIGA reactor operates in two basic modes: steady-state power levels up to 1.1 MW (thermal), and pulse operation with a step insertion of up to 2.8% $\Delta k/k$ ($4.00, when $\beta_{eff} = 0.007$) reactivity.

4.2 Reactor Core

The core forms a right cylinder consisting of a compact array of up to 87 standard TRIGA stainless steel-clad cylindrical fuel elements, three fuel-followed control rods, one transient control rod, control rod guides, and a startup neutron source and guide tube. The core is enclosed in a 0.1875 inch (0.4763 cm) thick aluminum shroud attached to the bottom of the core support adapter. Grid plates bolted to the top and bottom of the shroud secure the fuel elements, control rod guides, and neutron source guide tube. The active (i.e., fueled) reactor core is positioned within the shroud so that its horizontal center line is approximately 29 inches (73.66 cm) above the bottom of the reactor tank. Serial numbers inscribed on the core components identify individual fuel elements and control rods.

The AFRRI core initially consisted of 85 standard fuel elements, 2 instrumented fuel elements, 3 standard control rods, and 1 void-followed transient rod (87-3 core). In 1991, the 3 standard control rods were replaced with 3 fuel-followed control rods (FFCRs), and 2 standard fuel elements were replaced with 1 dry tube (CET) and 1 water hole in order

to maintain the k-excess below $5.00. In 1994, the void-followed transient rod was replaced with a poison-followed transient rod, and subsequently replaced with another void-followed transient rod. As fuel is consumed, the dry tube (CET) and water hole will be replaced with standard fuel elements.

The (87-3) core and the current core (85-3) components are listed in Table 4-1 and the current fuel burnup for each of the fuel elements is described in detail in Section 4.5.

Table 4-1 Core Components for 87-3 (Before FFCRs installation) and 85-3 (After FFCRs installation) Cores.

Core Configuration	Before FFCRs 87-3	After FFCRs 85-3
Standard Fuel Elements	85	83
Instrumented Fuel Elements	2	2
Standard Control Rods	3	
Fuel-followed Control Rods		3
Void-followed Transient Rod	1	1
Dry Tube (E23)		1
Water Hole (F9)		1
Total	91	91

4.2.1 Reactor Fuel

The AFRRI-TRIGA Mark-F reactor uses standard TRIGA stainless steel-clad, cylindrical fuel elements (Figure 4-1) in which the zirconium hydride moderator is homogeneously mixed with the enriched uranium fuel. The active part of each fuel element consists of a cylindrical rod of uranium-zirconium hydride containing 8.5 weight-percent uranium with less than 20 percent U^{235} enrichment.

The hydrogen-to-zirconium atom ratio of the fuel-moderator material is approximately 1.7 to 1. The nominal weight of U^{235} in each standard fuel element is [redacted] grams. The (b)(7)(F) uranium-zirconium hydride section is approximately [redacted] in length and [redacted] in diameter. A solid zirconium rod 0.225 inches (0.572 cm) in diameter and 15 inches (38.1 cm) in length is centered in the fuel region of each fuel element to provide structural support. Graphite end plugs, 3.44 inches (8.738 cm) in length, are located above and below the fuel-moderator section and serve as top and bottom axial reflectors.

Burnable poison (samarium) is included in each fuel element to minimize reactivity changes resulting from fission product buildup and fuel burnup. The burnable poison is mixed with aluminum to form wafers approximately 0.015 inch (0.0381 cm) thick. These wafers are located between the fuel moderator section and the graphite reflector end plugs.

The fuel moderator section, two graphite end plugs and burnable poison wafers are clad in 0.020 inch (0.0508 cm) Type 304 stainless steel. The rod is sealed at the top and bottom with stainless steel end fittings. An AFRRI-TRIGA fuel element is approximately (b)(7)(F) in length and weighs nearly (b)(7)(F) Up to 87 fuel elements (86 fuel elements if the CET is in place) may be loaded into the core lattice. The current core configuration utilizes 85 fuel elements.

In order to monitor the fuel temperature, two instrumented fuel elements (Figure 4-2) are placed in the core, one each in the B and C rings. An instrumented fuel element has three chromel-alumel thermocouples embedded in the fuel-moderator section at different axial locations. The tips of the thermocouples are located near the vertical axis of the fuel section. The center thermocouple is located at the midplane of the fuel section, and the other two thermocouples are located 1 inch (2.54 cm) above and below the center thermocouple. The thermocouple lead wires pass through a soft solder seal contained in the 0.5 inch (1.27 cm) outer diameter stainless-steel tube welded to the element's top end fixture. The instrumented fuel elements are identical to the standard fuel elements in all other respects.

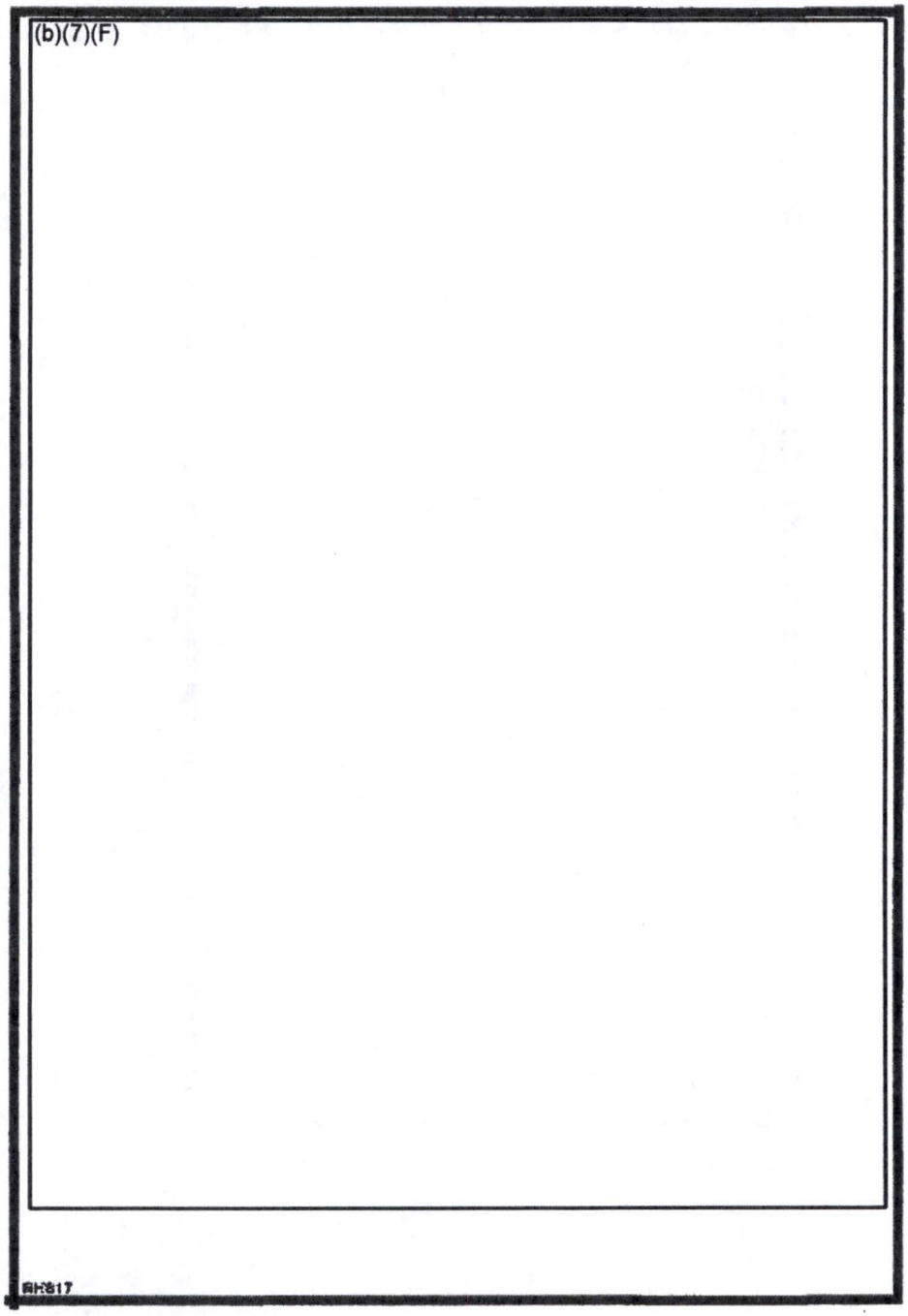

Figure 4-1 Standard fuel element

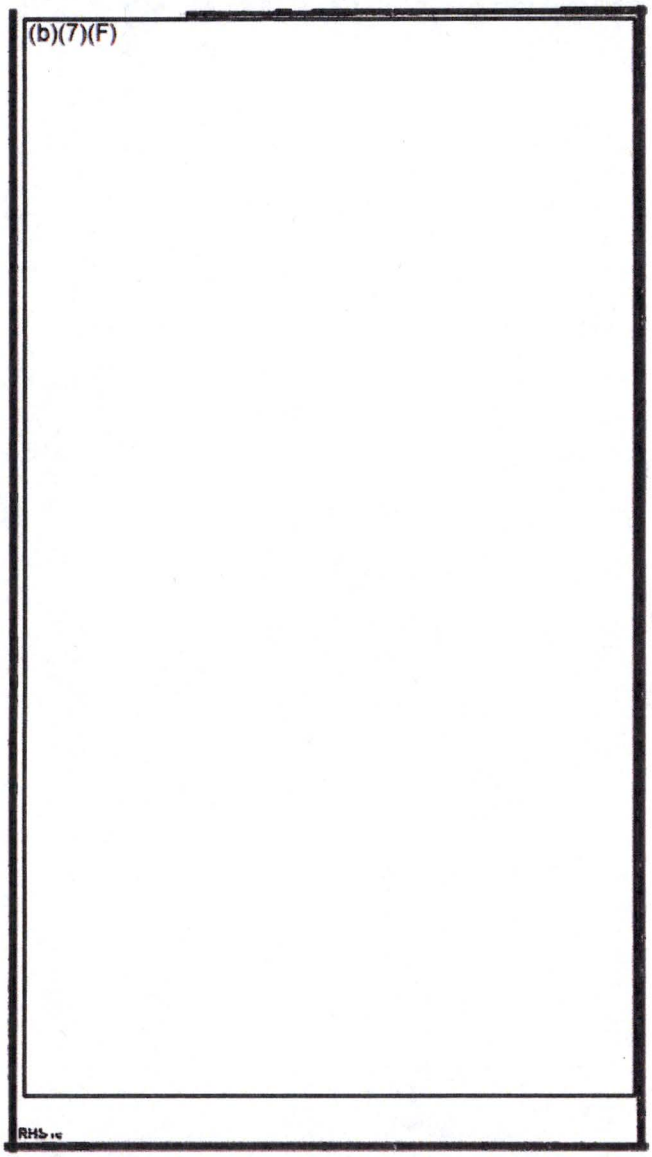

Figure 4-2 Instrumented fuel element

4.2.2 Control Rods

Reactor power in the AFRRI-TRIGA reactor is regulated by using three standard or fuel-followed control rods and one air-, aluminum-, or poison-followed transient control rod, all four of which contain neutron-absorbing material. Control rod movement within the core is accomplished using rack-and-pinion electromechanical drives for the standard control rods and a pneumatic-electromechanical drive for the transient control rod.

Three standard control rods were replaced with fuel-followed control rods (FFCRs) in 1991. The void-followed transient rod was replaced with a poison-followed transient rod in 1994, and subsequently replaced with another void-followed transient rod.

The reactivity worth of the individual rods is discussed in further detail in Section 4.5.

4.2.3 Neutron Moderator and Reflector

The core moderator consists of both water and zirconium hydride. The reactor core is reflected on the top and bottom by graphite end plugs in each fuel element, and at the periphery by water.

4.2.4 Neutron Startup Source

An americium-beryllium (Am-Be) neutron startup source (curies) is used in the AFRRI-TRIGA reactor. The Am-Be source produces neutrons by the (α,n) reaction: (b)(7)(F)

$$_{95}Am^{241} \rightarrow {}_{93}Np^{237} + {}_{2}\alpha^{4}\ (5.5\ MeV)$$

$$_{4}Be^{9} + {}_{2}\alpha^{4} \rightarrow [{}_{6}C^{13}]^{*} \rightarrow {}_{6}C^{12} + {}_{0}n^{1}$$

* Excited state; i.e., unstable

Americium-beryllium neutron sources are used for applications where small size and constant neutron strength over a relatively long useful life are desired. The Am-Be neutron startup source used in the AFRRI reactor yields approximately (b)(7)(F) neutrons per second per curie, consists of pelletized intimate mixtures of AmO_2Be in a weight ratio of 1 to 10, and is doubly encapsulated in Type 304L stainless steel.

The neutron source is inserted into the reactor core inside a 0.875 inch (2.223 cm) diameter tubular source guide tube (Figure 4-3). The neutron source guide tube is located in the upper grid plate (between F-22 and F-23) near the edge of the grid array. When bolted to the upper grid plate, the guide tube projects downward alongside of and just outside the fuel array. When the neutron source is inserted into the guide tube, the source material is positioned at the horizontal centerline of the core. The neutron source can be withdrawn from the guide tube for tests or storage by means of a cable attached to the top of the source holder.

4.2.5 Core Support Structure

A four-wheeled carriage, traveling on two tracks that span the reactor tank, is used to move the reactor core laterally from one operating position to another. In addition to supporting the core, the carriage also serves as a support for the four control rod drives, the N^{16} diffuser system (Section 5.6), various electronic devices, and core monitoring instrumentation.

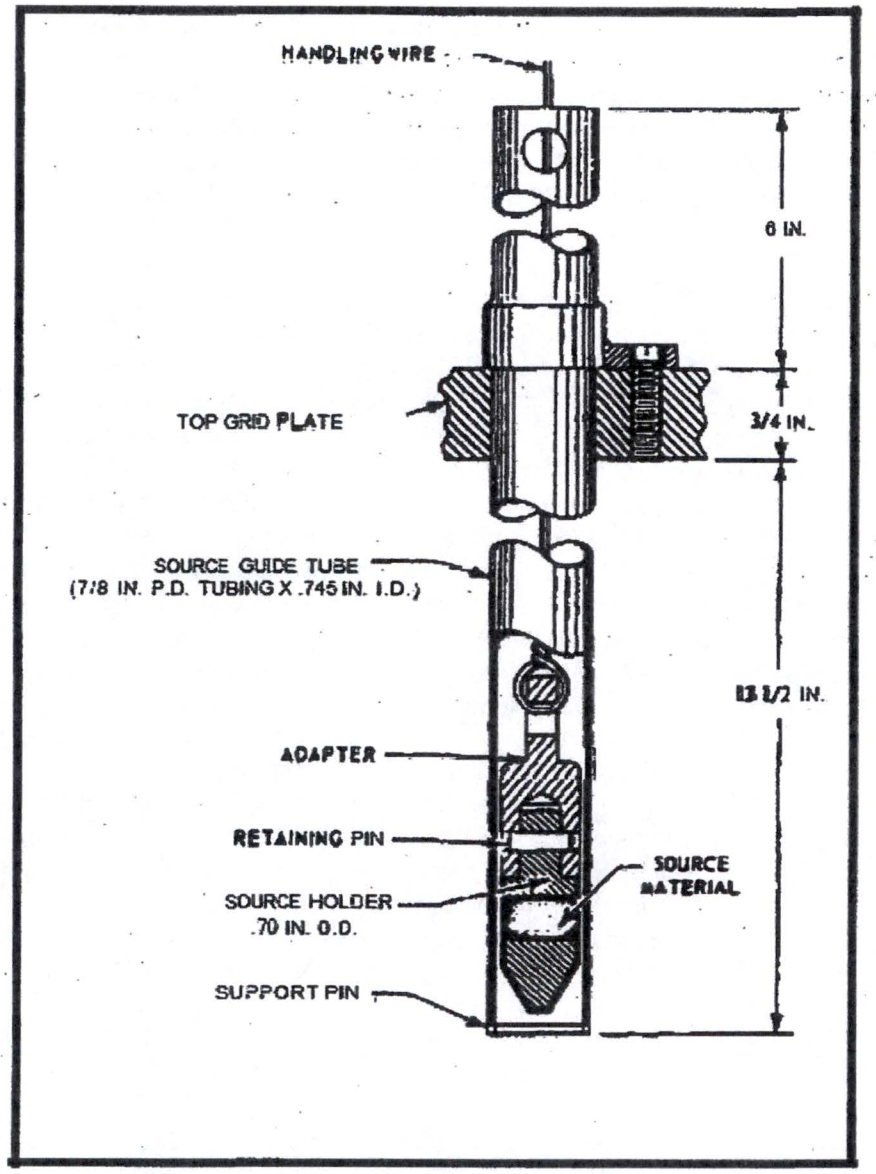

Figure 4-3 Neutron source and guide tube

The carriage consists of a structural steel framework enclosed by removable aluminum covers. Four control rod drives are attached to a mounting plate elevated above the carriage. Elevation of the control rod drives assures adequate clearance above the pool water surface and permits direct-line access to the core components and fuel elements. The wheels on one side of the carriage are grooved to match a double-beveled track. Engagement of the wheels and track, therefore, restrains any lateral displacement of the carriage. The two wheels on the opposite side of the carriage are flat-faced and roll on a flat track.

The carriage is propelled using a two-speed electric motor and a rack-and-pinion gear system. The gear rack is attached to the inside of the double-beveled track. The carriage is driven at two speeds, nominally 1.5 feet (45.72 cm) per minute and 2.25 feet (68.58 cm) per minute. Low speed is used during the first and last foot of travel as the carriage moves from one extreme limit to the other. The intervening distance is traversed at the higher speed. Microswitches are employed to automatically change the drive motor's speed, depending on the carriage's position on the track, and to stop the drive motor when the carriage has reached either of its two limits of travel. These switches also form part of the Facility Interlock System. As a safety measure, mechanical stops are mounted at both ends of the carriage track to prevent carriage overtravel at the limits. The carriage position is indicated on the reactor console. Precise repositioning of the carriage may require the use of reference marks on the carriage tracks. The variety of core carriage positions is broken down into three general regions. These regions are:

Region 1	The range of positions within 12 inches (30.48 cm) of the maximum travel distance of the core dolly carriage at ER #1
Region 2	The range of positions between Region 1 and Region 3, in which interference between the core shroud and the rotating reactor tank lead shield doors could occur
Region 3	The range of positions within 12 inches (30.48 cm) of the maximum travel distance of the core dolly carriage at ER #2.

Movement of the core carriage is initiated from the reactor console. Travel time for the carriage from one extreme position in the reactor tank to the other is approximately 5 minutes.

Power, control wiring, and compressed air are supplied to the carriage through cables and a flexible hose. The cables and hose are supported by a wall-mounted swinging boom. The swinging boom is attached to the carriage rod drive mounting pedestal. The swinging boom also supports the reactor room primary continuous air monitor (CAM) inlet hose and relieves stress on wiring and cables.

The core support structure consists of an aluminum cylinder approximately 36 inches (91.44 cm) in diameter and 12 feet (3.66 m) high, and an aluminum adapter 5 feet (1.52 m) high and 19.5 inches (49.53 cm) in diameter (Figure 4-4). Both the cylinder and adapter are formed from 0.3125 inch (0.7938 cm) thick aluminum plate. The cylinder connects the adapter to the core carriage. A vertical slot 16 inches (40.64 cm) wide extends the full height of the aluminum cylinder at its north side. This slot provides

access to the inside of the support structure, permitting the installation and removal of core components without raising them above the pool water level.

4.3 REACTOR TANK OR POOL

The reactor core is positioned in the reactor tank under approximately 15 feet (4.57 m) of demineralized water. The reactor tank water serves as radiation shielding, neutron moderator and reflector, and reactor coolant. The water purification and coolant systems which service the reactor pool water are discussed in Chapter 5.

The AFRRI-TRIGA reactor tank is constructed of aluminum and is embedded in ordinary concrete. The core is shielded in the radial directions by the reactor tank water and a minimum of (b)(7)(F) of ordinary concrete (with the exception of the exposure rooms). The vertical shielding consists of approximately 15 feet (4.857 m) of reactor tank water above the core and approximately (b)(7)(F) of ordinary concrete below the core separating the reactor tank from the subsoil underlying the reactor building. Aluminum was selected as the tank material to improve long-term reliability and to minimize problems of corrosion and neutron activation.

The reactor tank, which is cloverleaf-shaped, is approximately 19.5 feet (5.94 m) deep with a distance across the tank lobes of approximately 13 feet (3.96 m) (Figure 4-5). The basic wall thickness of the tank is (b)(7)(F), except for two cloverleaf projections that extend into the exposure rooms; this wall thickness is (b)(7)(F)
(b)(7)(F) The projections that extend into the exposure rooms allow the core to provide a 210° arc of radiation in the horizontal plane. The tank bottom and projection shelf thicknesses are (b)(7)(F) The exposure rooms are described in Section 10.2.

Since the core can be positioned at numerous horizontal locations within the reactor tank, it is possible to create a variety of radial reflector conditions. The radial reflector materials, made up of the following combinations of water, aluminum, and lead, with the core adjacent to Exposure Rooms #1 and #2 and at the middle of the reactor tank are (respectively):

- Effectively infinite thickness of water and 0.375 inches (0.9525 cm) of aluminum for 180°; 1 inch (2.54 cm) of water, 0.375 inches (0.9525 cm) of aluminum, 1 inch (2.54 cm) of water, 0.25 inches (0.635 cm) of aluminum, a cadmium-gadolinium shield (Section 10.2.1), and from 0 to 6 inches (15.24 cm) of lead for 180°

- Effectively infinite thickness of water and 0.375 inches (0.9525 cm) of aluminum for 180°; 1 inch (2.54 cm) of water, 0.375 inches (0.9525 cm) of aluminum, 1 inch (2.54 cm) of water, and 0.25 inches (0.635 cm) of aluminum for 180°

- Effectively infinite thickness of water and 0.375 inches (0.9525 cm) of aluminum for 360°

The axial reflector, both above and below the active core, remains unchanged for each of the above cases. It consists of the graphite end plugs in the fuel elements and the pool water above and below the core region.

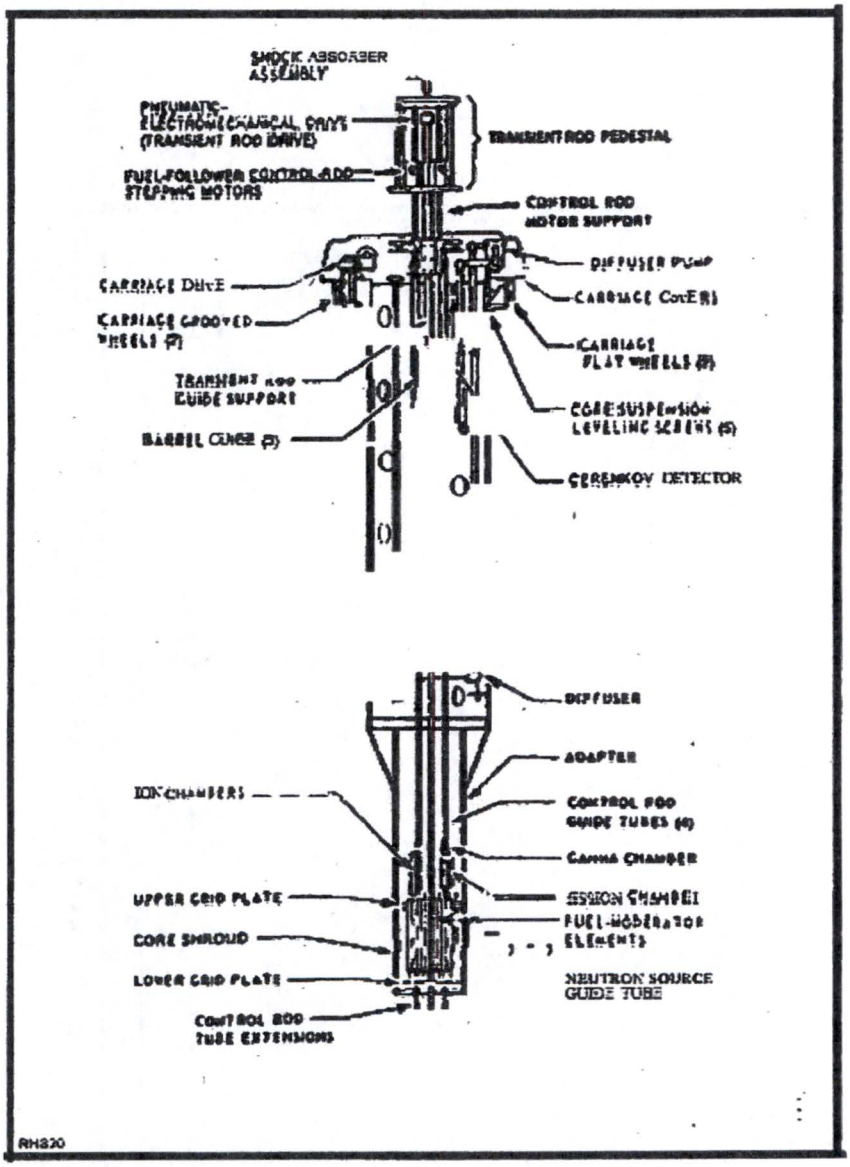

Figure 4-4 Support structure for AFRRI-TRIGA core

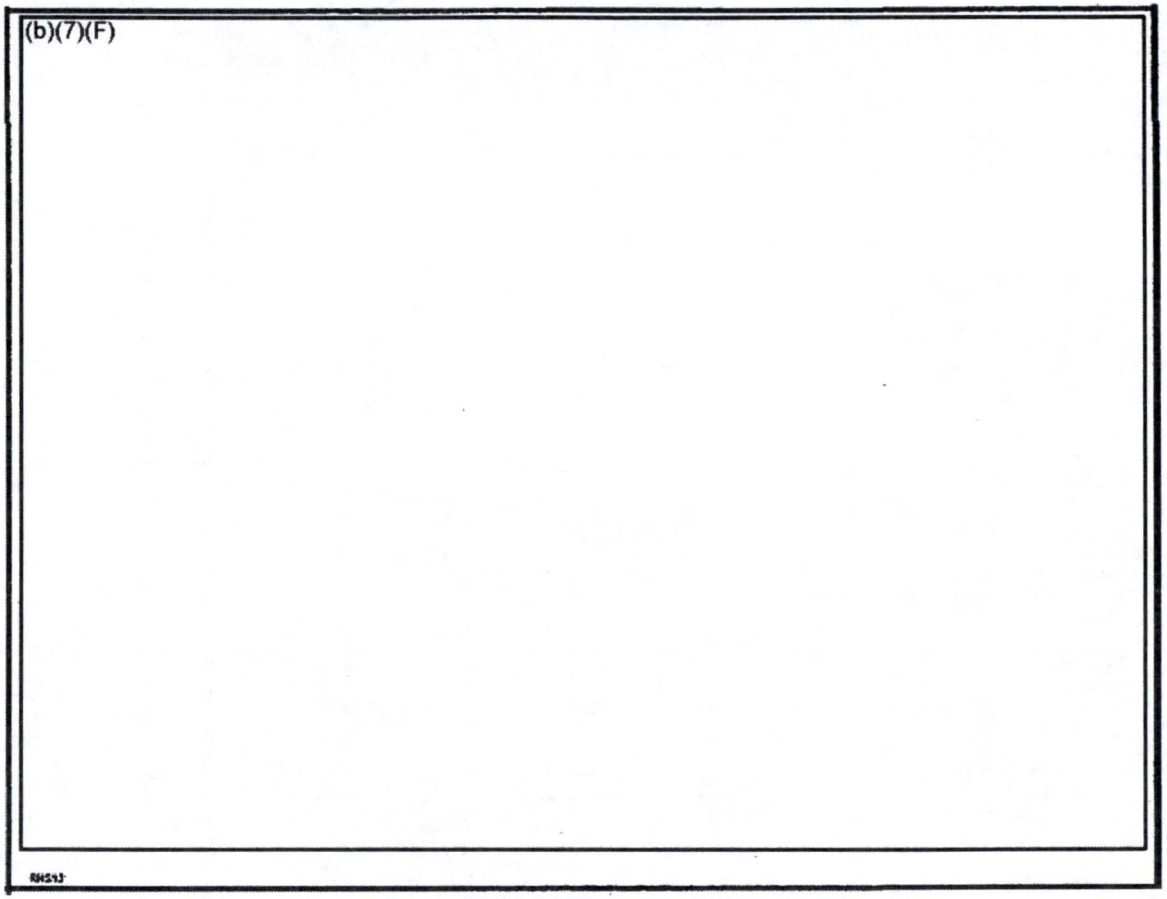

Figure 4-5 AFRRI-TRIGA Reactor Tank Plan

The reactor tank water level is monitored by a float-activated switch. A drop of approximately 6 inches (15.24 cm) in the reactor tank water level causes an immediate reactor scram and activates the following alarms:

- visual alarm on the reactor console
- audible (during non-duty hours) and visual alarm on the annunciator panel in Hallway 3101 (Section 7.7)

The reactor tank is illuminated by waterproof lights positioned along the wall of the reactor tank. Each lamp consists of a sealed-beam light enclosed in a waterproof housing and tube, suspended from the top edge of the reactor tank. The sealed tubing supporting the underwater lights is bent to prevent radiation streaming from the reactor tank.

4.4 BIOLOGICAL SHIELD

Two lead-filled radiation shield doors, shown in Figure 4-5, are located in the reactor pool and divide the reactor tank into two equal sections. The shield doors, when fully closed, allow access to one exposure room without significant radiation exposures while experiments are taking place in the other exposure room. The interlocking doors are constructed of 0.5-inch (1.27 cm) aluminum plate and 8-inch (20.32 cm) aluminum Z-sections. The doors are approximately 19 inches (48.26 cm) thick, 5 feet (1.524 m) high, and 6 feet (1.83 m) wide. Each watertight door is filled with approximately 18,000 pounds (8165 kg) of #6 lead shot and approximately 90 gallons (341 liters) of transformer oil to fill the gaps between the lead shot. The interlocking end pieces (Z-sections) of the shield doors are stepped to prevent radiation streaming between the doors when closed. Each door is supported on a low-friction thrust bearing mounted at the bottom of the tank. Pressurized air is supplied to the shield door bearings to minimize leakage of water into the shield door bearing housing.

The shield doors may be rotated 90° to permit the core support carriage to move from one end of the reactor tank to the other. Rotation of the doors is accomplished using a fractional horsepower drive motor with slip clutch located in a small pit at the top of the reactor tank. Power for door rotation is transmitted through a set of reduction gears. Each shield door is connected to a reduction gear mounted on the side of the carriage track by a vertical shaft extending from the top of each door. Approximately three minutes are required to fully open or close the lead shield doors.

Limit switches are used to indicate the fully opened or closed positions of the shield doors. These limit switches, located on top of the reduction gears, are part of the Facility Interlock System which prevents unintentional movement of the core support carriage into the mid-pool region unless the shield doors are fully opened and also denies power to the control rod magnets unless the shield doors are either fully opened or fully closed. The status of the shield doors is indicated on the reactor console and a ceiling-mounted TV camera in the reactor room provides an overhead view of the reactor tank to the operator in the control room.

4.5 NUCLEAR DESIGN

4.5.1 Calculation Models; Nuclear Analysis Codes

Three-dimensional calculations are performed using both diffusion theory and Monte Carlo codes. In general, multi-group diffusion theory is used for design calculations since it gives adequate results for systems of this kind and its multi-group fluxes and cross sections are easily utilized in nuclide burnup calculations. The Monte Carlo calculations are used to evaluate the facilities around the core and to compute the worth of core components in different core configurations.

The diffusion theory code utilized in this analysis is DIF3D, a multi-group code which solves the neutron diffusion equations with arbitrary group scattering (References 4-1 and 4-2).

The Monte Carlo code utilized in this analysis is MCNPX 2.6. MCNPX contains its own cross section library (Reference 4-3).

The BURP/DIF3D module, (Reference 4-4), is used for the burnup calculations with the cross section data generated with GGC-5, (Reference 4-5).

4.5.1.1 MCNPX Models

This section discusses the MCNPX models developed for these analyses and the benchmark calculations for the AFRRI core and determines nuclear parameters for various cores and the burnup-dependent parameters.

Reactor calculations were performed in three dimensions for the full core loading of the AFRRI 87-3 and 85-3 cores using the MCNPX, Version 2.6d, continuous energy Monte Carlo code. The plane view of the MCNPX model for the 87-3 core is shown in Figure 4-6a, and the axial view is shown in Figure 4-6b. Figures 4-7a and 4-7b show plane and axial views of the MCNPX model for the 85-3 core.

The nuclide cross sections were based on ENDF/B VII data included in the MCNPX data libraries. The material composition used in the MCNPX models is listed in Table 4-2, and the atomic number densities of the fresh fuel meat used in the MCNPX models are listed in Table 4-3.

4.5.1.2 Fuel Burnup

The AFRRI fuel burnup for the individual fuel elements is listed in Table 4-4, and the average burnup of the fuel elements in the current core is estimated as ~ 40.0 MWD.

To make a comparison between the measured core excess reactivity and the calculated excess reactivity as a benchmark case, the 8.5/20 fresh fuel was burned 100 days at 1.0 MW using the 85-3 core. The three-dimensional depletion calculations were performed with BURP/DIF3D codes, and the calculated excess reactivity and bias-corrected reactivity are shown in Figure 4-8.

The cross section data file for DIF3D calculations had 140 ppm of Hf in Zr built-in compared to 60 ppm per the manufacturer's data. The excess Hf in Zr yields approximately 0.64% Δk/k of excess reactivity in the burnup calculations with BURP with the Xe not removed. In actual operation, the buildup of Xe decayed during the shutdown period. Therefore, the straight burnup in the calculation without the periodic shutdown (ignoring the decaying Xe) would yield a fairly large bias. The Hf and Xe bias was estimated to be about 2.11% Δk/k.

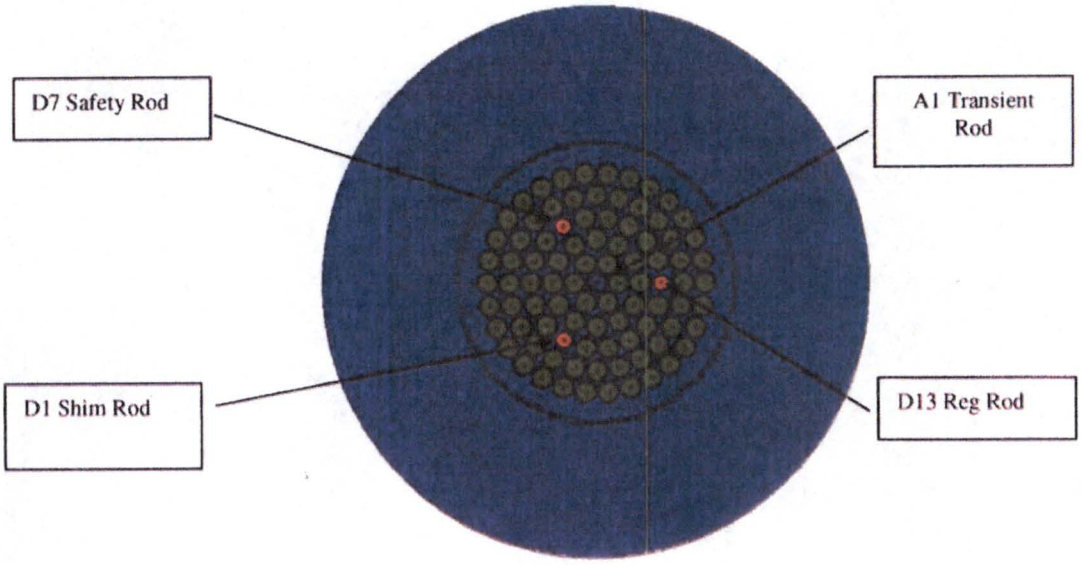

Figure 4-6a The plan view of the MCNPX Model for 87-3 Core.

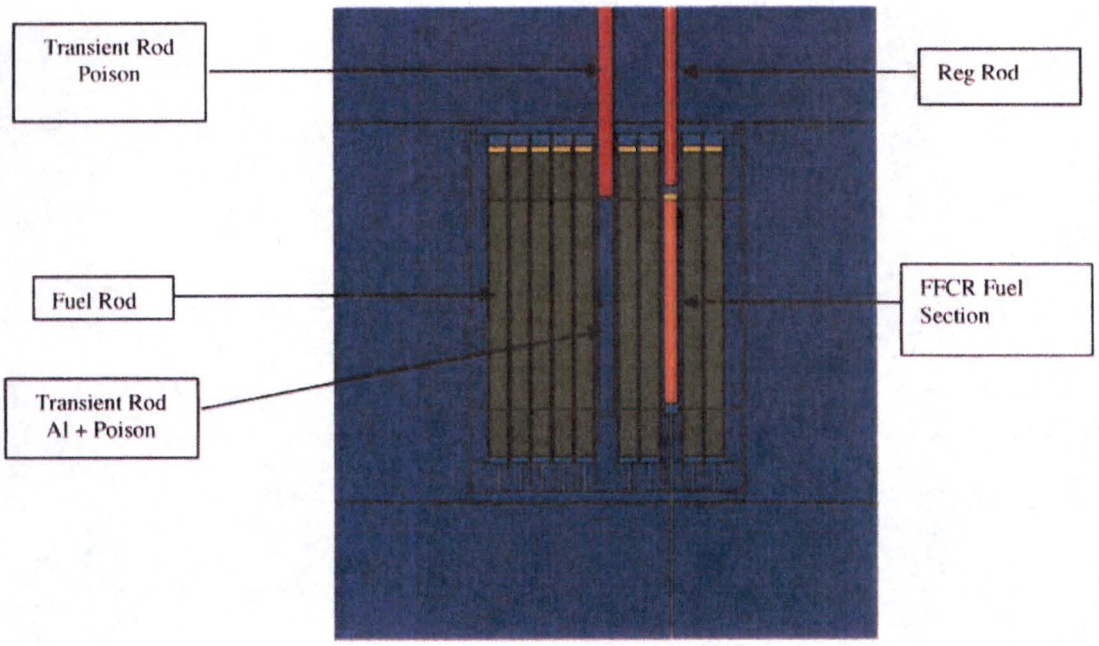

Figure 4-6b The axial view of the MCNPX Model for 87-3 Core.

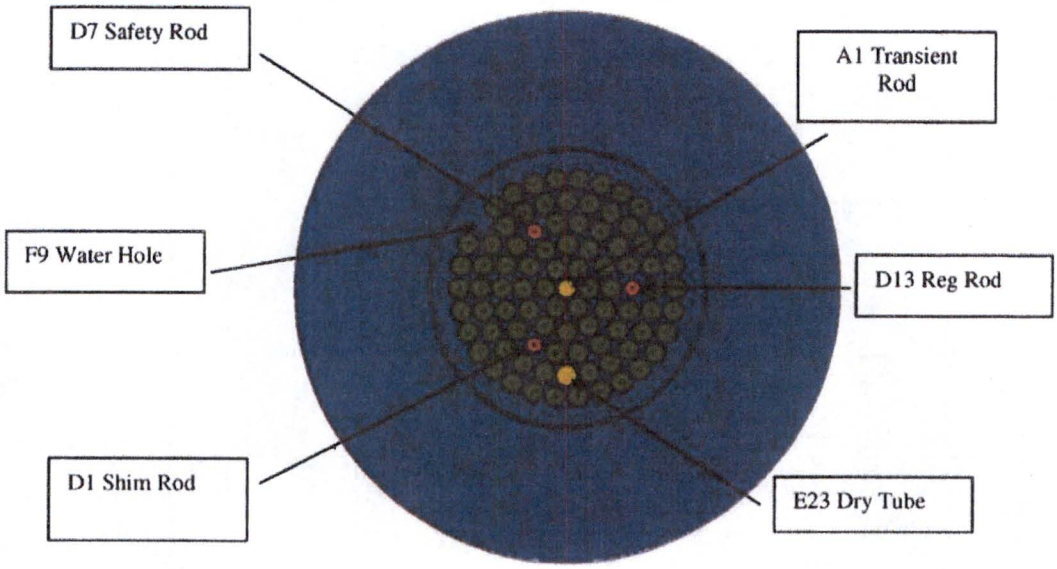

Figure 4-7a The plan view of the MCNPX Model for 85-3 Core

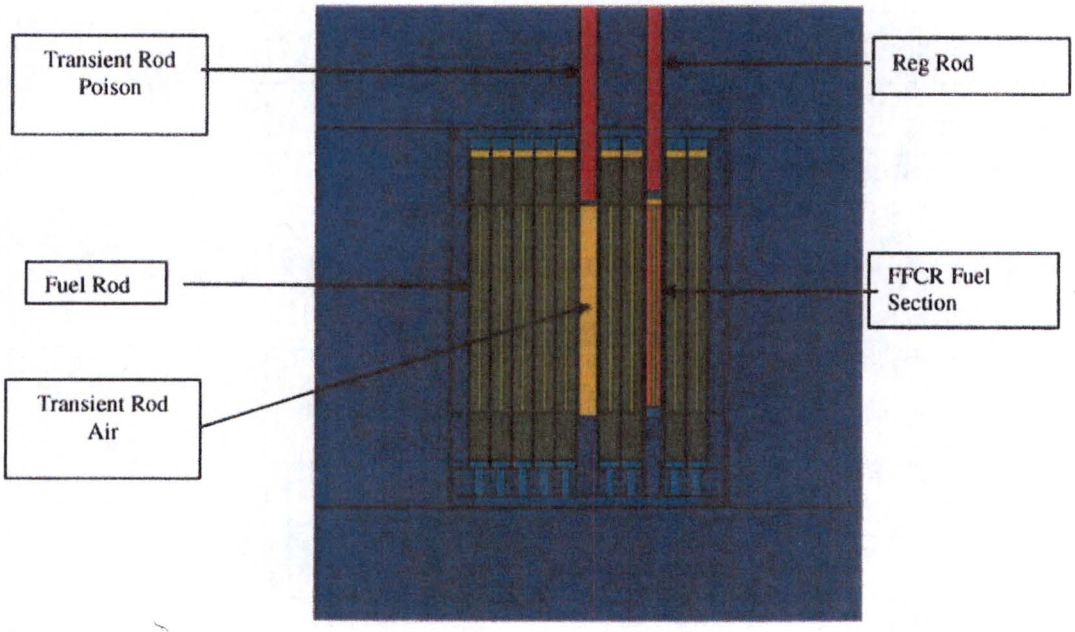

Figure 4-7b The axial view of the MCNPX Model for 85-3 Core

Table 4-2 Material Composition used in the MCNPX Models.

Material	Nuclide	Nuclide Density (atoms/b-cm)	Physical Density (g/cc)
SS 304 clad and fittings	Cr-50 Cr-52 Cr-53 Fe-56 Ni-58 Mn-55	7.780E-04 1.500E-02 1.701E-03 5.673E-02 7.939E-03 1.697E-03	7.98
Graphite Reflector In Fuel	C-12		1.556*
Zr Fuel Pin	Zr		(b)(7)(F)
Al 6061	Al-27 Fe-56	5.8693E-02 5.0200E-04	2.70
B_4C in Control Rods 90% of theoretical	B-10 B-11 C-12	2.095E-02 8.431E-02 2.632E-02	
Water	H-1 O-16		1.00
Air	N-16 O-16		1.23E-04

* Smeared density w/ gap, actual density is 1.75 g/cc
** Smeared density w/gap, actual density is 6.51 g/cc

Table 4-3 Number Densities of the Fuel Meat Used in the MCNPX Models.

	Number Density (atoms/b-cm)	
Nuclide	Standard and Instrumented Fuel Elements	Fuel-Followed Control Rod
(b)(7)(F)		
H-1	5.8598E-02	5.7778E-02
C-12	1.4827E-03	1.5238E-03
Zr	3.5551E-02	3.5116E-02
Hf	2.1331E-06	2.1069E-06
Sum	9.6902E-02	9.6268E-02

Table 4-4 The Fuel Burnup for Current Core (Avg. Burnup ~ 40 MWD)

CORE POSITION	BURNUP MWH	BURNUP MWD	CORE POSITION	BURNUP MWH	BURNUP MWD
B1	1007.5	42.0	E9	1008	42.0
B2	695.7	29.0	E10	1008	42.0
B3	1008	42.0	E11	1008	42.0
B4	1008	42.0	E12	1008	42.0
B5	280.4	11.7	E13	1008	42.0
B6	985.6	41.1	E14	1008	42.0
C1	1008	42.0	E15	1008	42.0
C2	738.5	30.8	E16	1008	42.0
C3	993.7	41.4	E17	1008	42.0
C4	993.7	41.4	E18	1008	42.0
C5	999.7	41.7	E19	963.6	40.2
C6	1008	42.0	E20	1008	42.0
C7	1008	42.0	E21	1008	42.0
C8	1008	42.0	E22	1008	42.0
C9	1008	42.0	E24	1007.5	42.0
C10	1008	42.0	F1	1008	42.0
C11	1008	42.0	F2	1008	42.0
C12	1008	42.0	F3	984.7	41.0
D1 (FFCR)	288.9	12.0	F4	874.8	36.5
D2	1008	42.0	F5	696.2	29.0
D3	746.4	31.1	F6	1008	42.0
D4	1008	42.0	F7	973.2	40.6
D5	890.6	37.1	F8	491.7	20.5
D6	1008	42.0	F10	1008	42.0
D7(FFCR)	296.9	12.4	F11	1008	42.0
D8	1008	42.0	F12	1008	42.0
D9	1008	42.0	F13	1008	42.0
D10	1008	42.0	F14	1008	42.0
D11	1008	42.0	F15	878.3	36.6
D12	1008	42.0	F16	1007.8	42.0
D13 (FFCR)	297.3	12.4	F17	1007.8	42.0
D14	1008	42.0	F18	1008	42.0
D15	1008	42.0	F19	1008	42.0
D16	1008	42.0	F20	1008	42.0
D17	997.9	41.6	F21	1008	42.0
D18	1008	42.0	F22	945.4	39.4
E1	696.2	29.0	F23	1008	42.0
E2	1008	42.0	F24	1008	42.0
E3	1008	42.0	F25	1008	42.0
E4	1008	42.0	F26	1008	42.0
E5	1008	42.0	F27	1008	42.0
E6	1008	42.0	F28	1008	42.0
E7	1008	42.0	F29	899.1	37.5
E8	1008	42.0	F30	1008	42.0

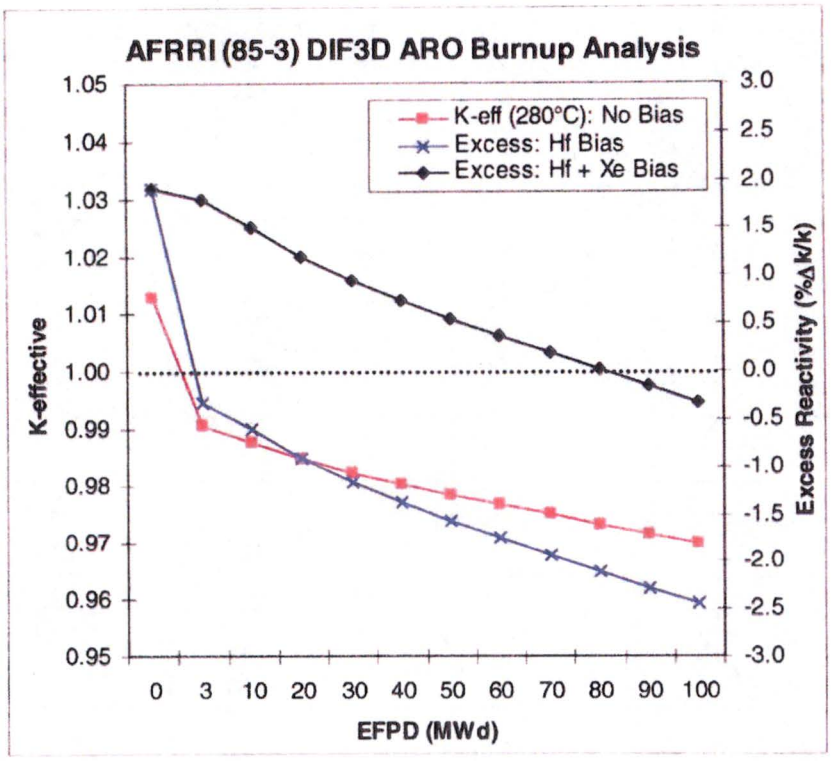

Figure 4-8 The excess reactivity as a function of burnup for 85-3 Core

4.5.2 Effective Delayed Neutron Fraction, β_{eff}

The effective delayed neutron fraction, β_{eff}, was derived from MCNPX calculations of the AFRRI cores with all control rods withdrawn.

The computed values for K_t and K_p are used in the following expression to obtain β_{eff}:

$$\beta_{eff} = 1 - [K_p / K_t]$$

Where: K_p = core reactivity using prompt fission spectrum only
K_t = core reactivity using prompt and delayed fission spectrum

The effective delayed neutron fractions were estimated using the above equation with MCNPX results for the 87-3 core with a poison-followed transient rod, the 85-3 core with a poison-followed transient rod, and the 85-3 core with a void-followed transient rod. Table 4-5 shows the calculated effective delayed neutron fractions. For the calculation, BOL fuel number densities were used and all control rods were withdrawn at 23°C.

The current core configuration is the third case in Table 4-5, and the calculated effective delayed neutron fraction at BOL is 0.0075 ± 0.0001.

Table 4-5 The Calculated Effective Delayed Neutron Fraction for various Core Configurations At BOL.

Core at BOL	Effective Delayed Neutron Fraction, β_{eff}
87-3 w/Poison-Followed Transient Rod	0.0078 ± 0.0002
85-3 w/Poison-Followed Transient Rod	0.0076 ± 0.0001
85-3 w/Void-Followed Transient Rod	0.0075 ± 0.0001

The burnup dependent delayed neutron fractions were calculated for the 85-3 core with a void-followed transient rod, and the results are shown in Table 4-6. The MOL case was calculated with the burnup (~ 40 MWD) number densities shown in Table 4-7 and, for the EOL case, 90 MWD burnup number densities from the BURP/DIF3D calculation were used.

The effective delayed neutron fraction decreases as the core burnup increases. The calculated effective delayed neutron fraction of 0.0075 ± 0.0001 at BOL decreases to 0.0068 ± 0.0001 at EOL.

Table 4-6 The Calculated Effective Delayed Neutron Fraction for 85-3 Core w/Void-Followed Transient Rod.

Core Lifetime	Effective Delayed Neutron Fraction, β_{eff}
BOL	0.0075 ± 0.0001
MOL	0.0070 ± 0.0001
EOL	0.0068 ± 0.0001

Table 4-7 The atomic density used for each individual fuel element in the 85-3 core at MOL (current core burnup, and the average burnup is ~ 40 MWD)

Nuclide	10MWD	20MWD	30MWD				
	B5	F8	B2	C2	D3	E1	F5
(b)(7)(F)							
Rh103	4.0353E-08	3.7588E-08	1.1954E-07	1.0719E-07	9.0074E-08	7.0945E-08	5.2739E-08
Xe131	3.5946E-08	3.3482E-08	1.0645E-07	9.5448E-08	8.0213E-08	6.3182E-08	4.6974E-08
Cs133	8.7899E-08	8.1866E-08	2.6052E-07	2.3357E-07	1.9625E-07	1.5455E-07	1.1487E-07
Nd143	7.7672E-08	7.2343E-08	2.2961E-07	2.0594E-07	1.7313E-07	1.3642E-07	1.0146E-07
Pm147	2.9203E-08	2.7111E-08	8.5635E-08	7.6811E-08	6.4588E-08	5.0907E-08	3.7879E-08
Sm149	9.8482E-09	9.3367E-09	1.6736E-08	1.6185E-08	1.5222E-08	1.3700E-08	1.1624E-08
Sm151	5.3057E-09	4.9472E-09	1.4710E-08	1.3336E-08	1.1366E-08	9.0944E-09	6.8557E-09
H	5.8598E-02	5.8598E-02	5.8598E-02	5.8598E-02	5.8598E-02	5.8598E-02	5.8598E-02
C	1.4827E-03	1.4827E-03	1.4827E-03	1.4827E-03	1.4827E-03	1.4827E-03	1.4827E-03
Zr	3.5551E-02	3.5551E-02	3.5551E-02	3.5551E-02	3.5551E-02	3.5551E-02	3.5551E-02
Hf	2.1300E-06	2.1300E-06	2.1300E-06	2.1300E-06	2.1300E-06	2.1300E-06	2.1300E-06
Total	9.6901E-02	9.6901E-02	9.6899E-02	9.6899E-02	9.6899E-02	9.6900E-02	9.6900E-02

Nuclide	40 MWD					10 MWD
	B	C	D	E	F	FFCR
(b)(7)(F)						

* The fuel burnup numbers in the above table were rounded from the actual burnup numbers shown in Table 4-4.

** B, C, D, E, F represent all other fuel locations excluding B5, F8,B2,C2,D3, E1, and F5.

4.5.3 The Core Excess Reactivity

The core excess reactivities calculated with MCNPX for three different cores, an 87-3 core with a poison-followed transient rod, an 85-3 core with a poison-followed transient rod, and an 85-3 core with a void-followed transient rod at 23°C and BOL, are shown in Table 4-8.

The calculated burnup-dependent core excess reactivity for an 85-3 core with a void-followed transient rod and measured excess reactivity for the current core at 23°C are shown in Table 4-9. The measured value is \$4.37 and the calculated-with-MCNPX value is \$4.89 ± 0.01.

Table 4-8 The Calculated BOL Core Excess Reactivity for Various Core Configurations at 23°C.

Core at BOL	MCNPX k_{eff}	Core Excess Reactivity (\$)
87-3 w/Poison-Followed Transient Rod	1.04369 ± 0.00017	5.38 ± 0.02
85-3 w/Poison-Followed Transient Rod	1.03521 ± 0.00008	4.77 ± 0.01
85-3 w/Void-Followed Transient Rod	1.04761 ± 0.00004	6.03 ± 0.01

Table 4-9 The Calculated Core Excess Reactivity for an 85-3 Core w/ Void-Followed Transient Rod at 23°C.

Core Lifetime	MCNPX k_{eff}	MCNPX Core Excess Reactivity (\$)	Measured Core Excess Reactivity (\$)
BOL	1.04761 ± 0.00004	6.03 ± 0.01	
MOL	1.03521 ± 0.00008	4.89 ± 0.01	4.37
EOL	1.02126 ± 0.00008	2.99 ± 0.01	

4.5.4 The Control Rod Worth and Shutdown Margin (SDM)

The individual control rod worths for an 85-3 core with a void-followed transient rod for various time points were calculated with MCNPX, and the results are listed in Table 4-10. The transient rod has the highest worth among the four control rods.

The shutdown margin (SDM) for the 85-3 core is estimated to be the core excess reactivity minus total rod worth with the highest worth rod removed. The shutdown margin values are well below the Technical Specification limit of -$0.50.

Table 4.10 The Calculated Control Rod Worth ($) and Shutdown Margin for the 85-3 Core

Control Rod	MCNPX Control Rod Worth ($)		
	BOL	MOL	EOL
Shim	2.76 ± 0.04	2.96 ± 0.02	2.85 ± 0.02
Safety	2.94 ± 0.03	3.24 ± 0.02	3.08 ± 0.02
Regulating	3.02 ± 0.03	3.35 ± 0.02	3.18 ± 0.02
Transient	4.18 ± 0.03	4.63 ± 0.02	4.74 ± 0.02
Core Excess	6.03 ± 0.01	4.89 ± 0.01	2.99 ± 0.01
Total - Transient	8.72 ± 0.06	9.55 ± 0.03	9.11 ± 0.03
SDM	-2.69	-4.66	-6.12

4.5.5 Prompt Neutron Lifetime (ℓ)

The prompt neutron lifetime, ℓ, was computed by the 1/v absorber method, where a very small amount of boron is distributed homogeneously throughout the system and the resulting change in reactivity is related to the neutron lifetime. This calculation was performed using the 3-D diffusion theory model for the core to allow very tight convergence of the problem. The boron cross sections used in the core were generated over a homogenized core spectrum. Boron cross sections used in all other zones were generated over a water spectrum.

The neutron lifetime, ℓ , is defined as follows:

$$\ell = \Delta k_{eff}/\omega$$

Where Δk_{eff} is the change in reactivity due to the addition of boron and ω is related to the boron atom density and,

$$N_B = \omega/\delta_o v_o = 6.0205 \times 10^{-7}$$

where N_B = boron density (atoms/b-cm)
ω = integer = 100 (the calculation is insensitive to changes in ω between 1 and 100),
v_o = 2200 m/sec,
δ_o = 755 barns = δ_a^B at 2200 m/sec

As described in the β_{eff} section above, the 3-D model used very tight convergence criteria (1.0×10^{-8} of k_{eff}, 1.0×10^{-6} point flux). The cases were run cold (23°C) with fresh 8.5/20 fuel (BOL). The result for prompt neutron lifetime in the 85-3 core at BOL is:

$$\ell = 41.4\ \mu sec$$

The calculated prompt neutron lifetimes for BOL and EOL are listed in Table 4-11.

Table 4-11 The Calculated Prompt Neutron Lifetime for BOL and EOL in the 85-3 Core.

Core Lifetime	Prompt Neutron Lifetime (μsec)
BOL	41.4
EOL	39.5

4.5.6 Void Coefficient

The void coefficient of reactivity is defined for a TRIGA reactor as the negative reactivity per 1% void in the reactor core water. For the AFRRI 85-3 core, the calculated void coefficient is about 0.080% Δk/k per 1% water void. This void coefficient is not normally considered a safety concern for TRIGA reactors. The reason is the relatively small size of this coefficient and the fact that all TRIGA reactors are significantly under-moderated. Therefore, if a portion of the core water is replaced with a low density material (i.e., steam, gas including air, etc.), a negative reactivity will occur. An example would be placing a dry, experimental tube, with a void volume of 205 cc in the 38.1 cm core fueled height, in the central region of the core (replacing a fuel rod) and then being accidentally flooded with water. The calculated loss in core reactivity would be about $0.10 ± 0.03. A safety effect of rapid reactivity insertion to be considered is the effect of accidental flooding of an in-core dry experimental tube such as postulated above. In this case, the rapid reactivity insertion would be approximately $0.10. The insertion of $0.10 reactivity is far less than $1.00 (prompt critical).

The conclusion is that the very small void coefficient of reactivity is not a source of safety concern.

4.5.7 Prompt Negative Temperature Coefficient

The definition of α, the prompt negative temperature coefficient of reactivity, is given as:

$$\alpha = \frac{d\rho}{dT}$$

where ρ = reactivity = (k-1)/k
T = reactor temperature (°C)

$$\alpha = \frac{1}{k^2}\frac{dk}{dT}$$

To evaluate ($\Delta\rho$) from reactivity as a function of reactor core temperature, the finite differences can be written as follows:

$$\Delta\rho_{1,2} = \frac{k_2 - 1}{k_2} - \frac{k_1 - 1}{k_1}$$

$$= \frac{k_2 - k_1}{k_1 k_2}$$

Thus,
$$\alpha_{1,2} \cong \frac{k_2 - k_1}{k_1 k_2} \times \frac{1}{\Delta T_{1,2}}$$

The data in Tables 4-12 and 4-13 were produced from the calculations with DIF3D for the listed core temperatures.

Figures 4-9 and 4-10 show the prompt negative temperature coefficients for the 85-3 core at BOL and EOL as a function of reactor temperature.

Table 4-12 Reactivity Change with Temperature, 85-3 Core at BOL

Avg. Core Temp. (°C)	k_{eff}	Δk_{eff}	$\frac{k_a - k_b}{k_a \cdot k_b}$	$\alpha_{a,b}$
23	1.03923			
111.5		0.01669	0.01570	8.87E-05
200	1.02255			
240.0		0.00963	0.00930	1.16E-04
280	1.01292			
340.0		0.01483	0.01466	1.22E-04
400	0.99809			
550.0		0.03317	0.03444	1.15E-04
700	0.96493			
850.0		0.02769	0.03061	1.02E-04
1000	0.93724			

Table 4-13 Reactivity Change with Temperature, 85-3 Core at EOL

Avg. Core Temp. (°C)	k_{eff}	Δk_{eff}	$\frac{k_a - k_b}{k_a \cdot k_b}$	$\alpha_{a,b}$
23	0.99477			
111.5		0.01568	0.01609	9.09E-05
200	0.97909			
240.0		0.00900	0.00948	1.18E-04
280	0.97009			
340.0		0.01350	0.01455	1.21E-04
400	0.95659			
550.0		0.02925	0.03297	1.10E-04
700	0.92734			
850.0		0.02401	0.02867	9.56E-05
1000	0.90332			

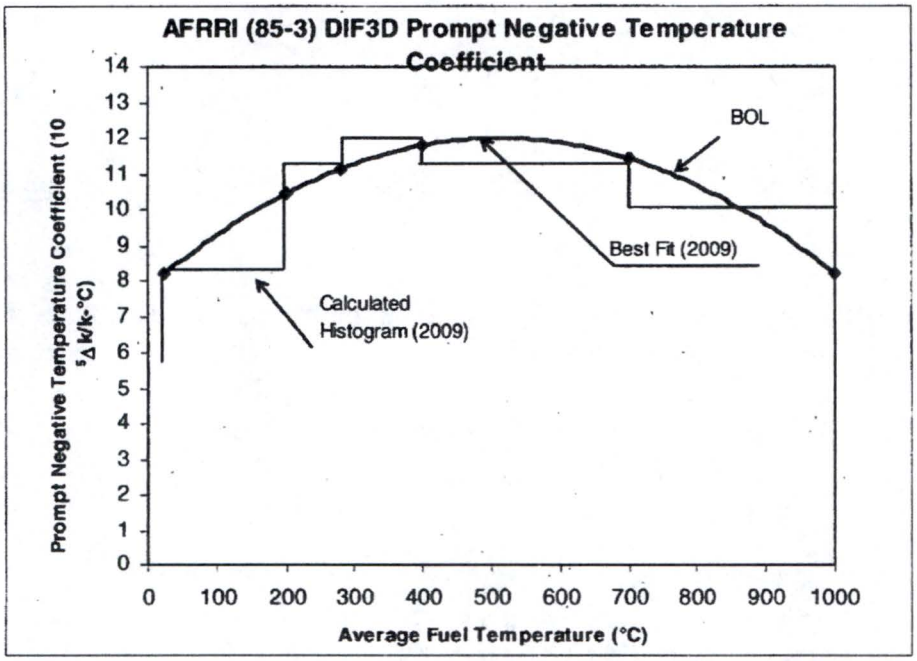

Figure 4-9 The Calculated Negative Temperature Coefficients for 85-3 Core at BOL.

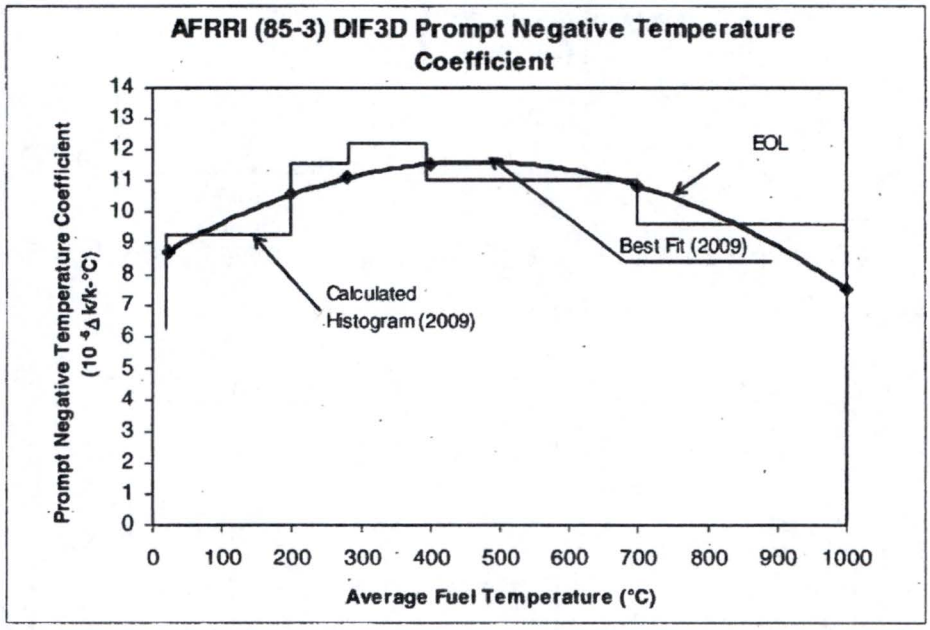

Figure 4-10 The Calculated Negative Temperature Coefficients for 85-3 Core at EOL

4.5.8 Power Peaking

The rod power factors for the 85-3 core were evaluated using DIF3D calculations at BOL and EOL. The results are shown in Table 4-14. The B-4 (B04 in Table) location shows the highest power factor for both BOL and EOL.

As the burnup increases, the rod power factors in the B, C, and D rings decrease slightly, and the rod power factors in the E and F rings increase. This is due to the flux depression as the U^{235} in the hot regions (B, C, and D rings) burns faster than in the outer regions.

4.5.9 Pulse Results

A calculation procedure (TRIGA-BLOOST) based on a space-independent kinetics model, Reference 4-8, has been developed for predicting pulse performance of TRIGA reactors.

The following simplified relationships are given to show qualitatively how the pulsing performance is influenced by the important reactor parameters:

$$\tau = \ell / \Delta k_p = \text{Reactor period}$$

$$\overline{\Delta T} = \frac{2\Delta k_p}{\alpha} = E/C$$

$$\hat{P} = \frac{C(\Delta k_p)^2}{2\alpha\ell} = \text{Peak pulse power}$$

$$E = \frac{2C\Delta k_p}{\alpha} = \text{Total energy release in prompt burst}$$

Where:

ℓ = prompt neutron life

α = prompt negative temperature coefficient

C = total heat capacity of the core available to the prompt pulse energy release

$\overline{\Delta T}$ = change in average core temperature produced by the prompt pulse

Δk_p = that portion of the step reactivity insertion which is above prompt critical

Table 4- 14 The Rod Power Factors for the 85-3 core at BOL and EOL.

Location	BOL	EOL	Location	BOL	EOL
B01	1.525	1.494	E09	0.907	0.913
B02	1.534	1.502	E10	0.913	0.920
B03	1.543	1.509	E11	0.921	0.927
B04	1.552	1.517	E12	0.929	0.935
B05	1.547	1.513	E13	0.934	0.939
B06	1.531	1.499	E14	0.935	0.940
C01	1.392	1.374	E15	0.933	0.939
C02	1.397	1.378	E16	0.933	0.939
C03	1.403	1.383	E17	0.938	0.944
C04	1.405	1.384	E18	0.924	0.931
C05	1.424	1.402	E19	0.913	0.920
C06	1.427	1.404	E20	0.902	0.910
C07	1.435	1.412	E21	0.885	0.893
C08	1.435	1.412	E22	0.890	0.899
C09	1.438	1.416	E24	0.888	0.897
C10	1.414	1.393	F01	0.657	0.671
C11	1.392	1.372	F02	0.664	0.679
C12	1.374	1.356	F03	0.670	0.685
D01	1.033	1.027	F04	0.673	0.688
D02	1.182	1.178	F05	0.673	0.687
D03	1.181	1.177	F06	0.668	0.682
D04	1.181	1.176	F07	0.659	0.673
D05	1.175	1.170	F08	0.721	0.734
D06	1.186	1.179	F10	0.723	0.735
D07	1.063	1.052	F11	0.665	0.677
D08	1.212	1.205	F12	0.677	0.690
D09	1.214	1.206	F13	0.687	0.700
D10	1.220	1.212	F14	0.694	0.707
D11	1.221	1.213	F15	0.699	0.712
D12	1.229	1.221	F16	0.701	0.714
D13	1.085	1.074	F17	0.702	0.715
D14	1.213	1.207	F18	0.702	0.715
D15	1.188	1.183	F19	0.700	0.713
D16	1.165	1.161	F20	0.698	0.711
D17	1.142	1.140	F21	0.696	0.709
D18	1.149	1.146	F22	0.692	0.706
E01	0.886	0.895	F23	0.688	0.702
E02	0.891	0.900	F24	0.682	0.696
E03	0.896	0.905	F25	0.674	0.689
E04	0.899	0.908	F26	0.664	0.679
E05	0.896	0.904	F27	0.657	0.672
E06	0.887	0.895	F28	0.684	0.698
E07	0.933	0.939	F29	0.682	0.696
E08	0.921	0.927	F30	0.652	0.667

Water-filled regions within the core promote flux peaking and result in increased power peaking and peak fuel temperatures, especially during a reactivity pulse.

The BLOOST pulsing performance results have been prepared for the 85-3 Core at BOL, and the results are shown in Table 4-15.

Table 4-15 BLOOST Results for the Various Pulses at BOL

Parameter	$1.50	$1.60	$2.00	$3.00	$4.00
Peak Pulse Power (MW)	109	176	605	2609	4424
Energy Release (MJ)	6.1	8.1	15.3	31.5	43.1
Peak Fuel Temp (°C)	185	243	382	662	831
IFE Temp (°C)	151	189	308	530	666

4.6 Functional Design of the Reactivity Control Systems

4.6.1 Standard Control Rods and Guide Tubes

The shim rod (SHIM), safety rod (SAFE), and regulating rod (REG) constitute the three standard control rods and are located in core positions D-1, D-7, and D-13, respectively (Figure 4-11).

A standard control rod consists of a sealed stainless-steel tube (0.020 inch thick) approximately 38 inches (96.52 cm) long and 1.125 inches (2.858 cm) in diameter. The upper 4.75 inches (12.065 cm) of the rod is an air-filled extension section. The middle section (15 inches (38.1 cm)) of the rod contains a boron compound (25 percent free boron or boron compounds) as the neutron absorber, or poison.

The lower 14.875 inches (37.783 cm) of the rod (the follower) can contain a 12 wt% U-ZrH fuel mixture with a solid zirconium rod (0.225 inch diameter (0.572 cm)) in the center, a void follower, or a solid aluminum follower. The control rod guide tubes provide space for inserting and withdrawing the control rods, pass through the upper and lower grid plates, and are attached to the lower grid plate.

Figure 4-11 Upper and Lower Grid Plates

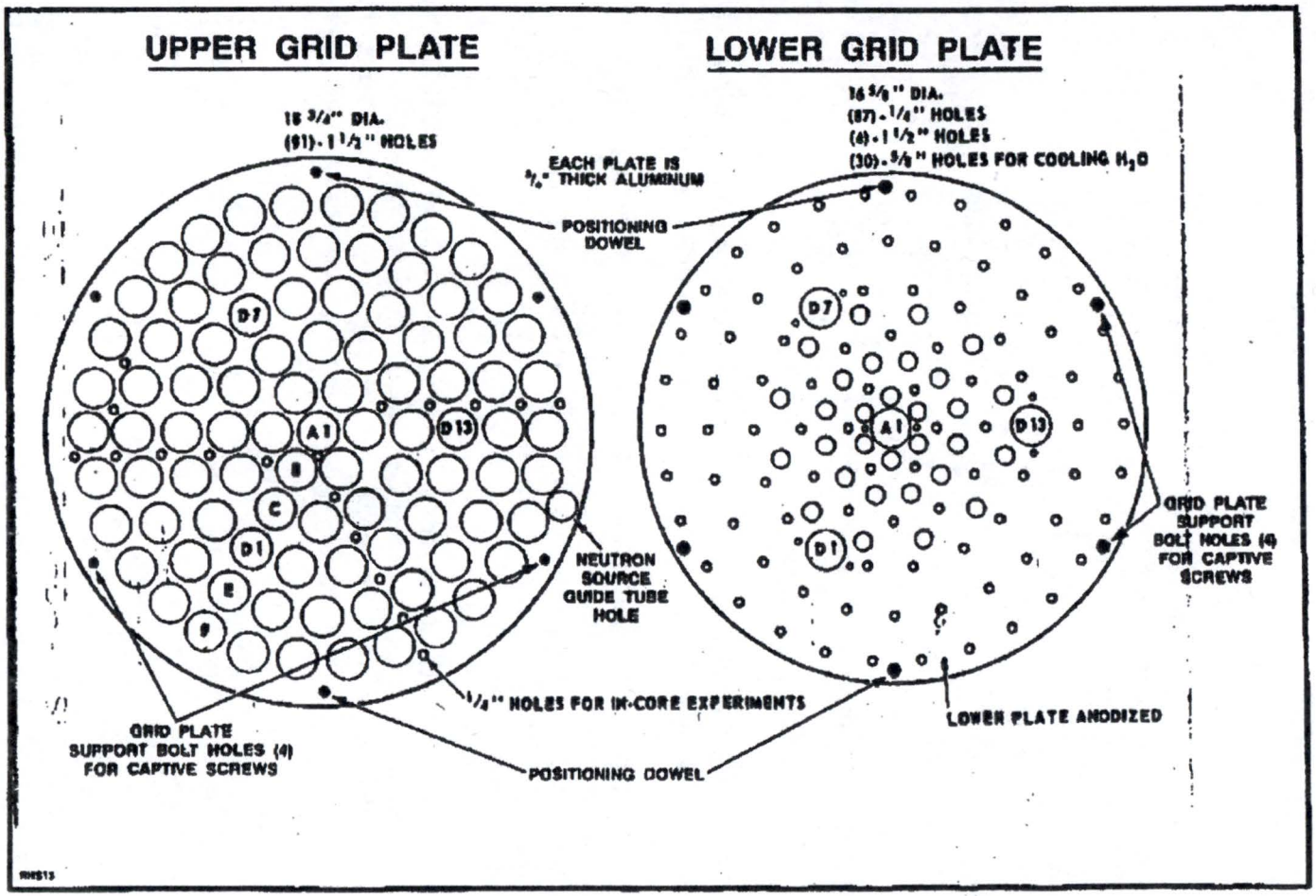

4.6.2 Standard Control Rod Drives

Rack-and-pinion electromechanical drive mechanisms (Figure 4-12), referred to as standard control rod drives, are used to change the positions of the shim, safety, and regulating rods.

The standard drive consists of a stepping motor, a magnetic coupler, a rack-and-pinion gear system, and a potentiometer used to provide an indication of rod position, which is displayed on the reactor console.

The pinion gear engages a rack attached to a draw tube supporting an electromagnet. The magnet engages the end of a long connecting rod. The connecting rod is attached at its lower end to the control rod. The magnet, its draw tube, and the upper portion of the connecting rod are housed in a tubular barrel. The barrel extends below the reactor pool water surface.

The lower end of the barrel acts as a mechanical stop limiting the downward travel of the control rod assembly. A piston with a Teflon seal is attached to the upper portion of the connecting rod. Since the upper portion of the barrel is well ventilated by slotted vents, the piston moves freely in this range but when the piston is within two inches of the bottom of its travel, its movement is dampened by the dashpot action of the graded vents in the lower end of the barrel. This dashpot action reduces bottoming impact during a scram.

When the stepping motor is energized, the pinion gear shaft rotates, thus raising the magnet draw tube. When the electromagnet, attached to the draw tube, is in contact with the connecting rod and energized, the connecting rod rises, withdrawing the control rod from the reactor core. When the reactor is shut down (scrammed), the electromagnet is de-energized, releasing the connecting rod. The connecting rod and the control rod then drop by gravitational force, reinserting the neutron poison into the core.

A ROD DOWN microswitch indicates when the control rod is at its lower limit of travel, i.e., fully inserted into the core. A foot plate, which projects through a slot in the barrel, is attached to a spring-loaded pull rod that extends vertically up through the drive mount. An adjustable fixture on the upper end of the push rod engages the actuating lever of the ROD DOWN microswitch.

A second microswitch, the DRIVE UP microswitch, is used to indicate the full up position and stop the movement of the electromagnet (drive) when it reaches its upper limit of travel. When the magnet draw tube is raised to its upper limit, the upper surface of the magnet contacts a push rod which extends vertically up through the drive mount. An adjustable fixture on the upper end of the push rod engages the actuating lever of the DRIVE UP microswitch.

A third microswitch, the DRIVE DOWN microswitch, is actuated when the electromagnet (drive) is at its lower limit. When the magnet reaches its lower limit, a rigid adjustable fixture at the upper end of the draw tube engages the actuating lever of the DRIVE DOWN microswitch, which stops the movement of the electromagnet (drive).

The reactor interlock system prevents the simultaneous manual withdrawal of two or more standard control rods during steady-state modes of operation and prevents the withdrawal of any standard control rod during pulse operation.

Figure 4-12 Standard Control Rod Drive

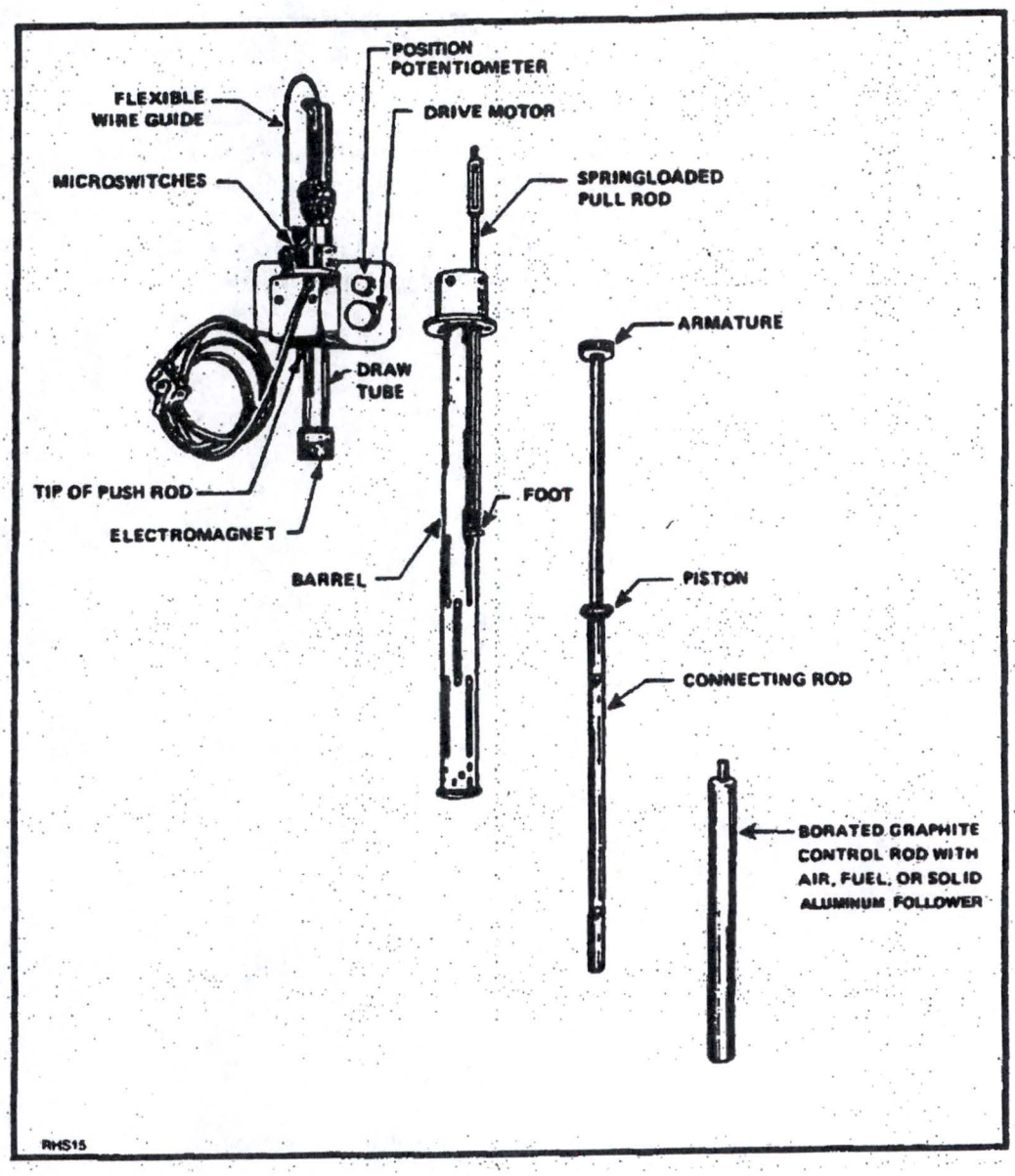

4.6.3 Transient Control Rod

A fourth control rod, the transient rod, consists of a sealed aluminum tube of slightly larger diameter than a standard control rod (Figure 4-14). It is located in core position A-1. The upper section (15 inches (38.1 cm)) of the rod is filled with a boron compound (25 percent free boron or boron compounds).

The lower portion of the rod contains a machined solid aluminum follower, a combined poison and aluminum (4 percent total boron to total atom ratio) follower, or an air follower. The transient rod operates in a guide tube identical to those used for the standard control rods. Both the standard control rods and the transient rod have a maximum travel of 15 inches (38.1 cm). When the control rods are at their upper limits of travel, the center neutron poison section of each rod is slightly above the fueled or active region of the core.

Figure 4-13 Transient Rod Drive Mechanism

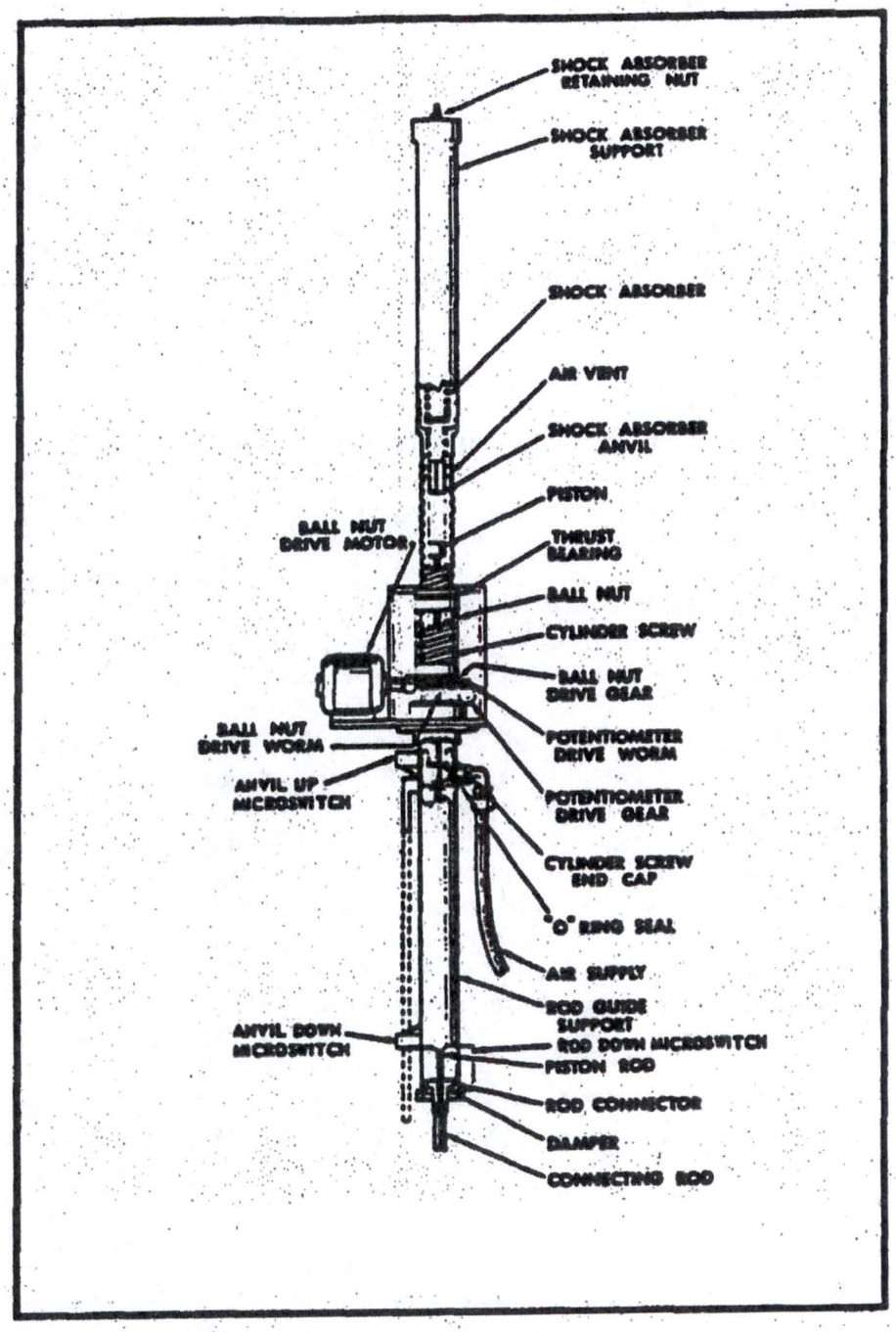

4.6.4 Transient Rod Drive

The AFRRI-TRIGA reactor is equipped with a pneumatic-electromechanical drive system for the transient control rod (Figure 4-13).

The pneumatic-electromechanical drive, referred to as the transient rod drive, is a single-acting pneumatic cylinder system. A piston within the cylinder is attached to the transient control rod by means of a connecting rod. The piston rod passes through an air seal at the lower end of the cylinder. For pneumatic operation, compressed air, admitted at the lower end of the cylinder, is used to drive the piston upward. As the piston rises, the air being compressed above the piston is forced out through vents at the upper end of the cylinder. At the end of its stroke, the piston strikes the anvil of a shock absorber and is decelerated at a controlled rate during its final inch of travel. This action minimizes rod vibration when the piston reaches its upper limit stop. Adjustment of the anvil's position, i.e., the volume of the cylinder, controls the piston's stroke length and hence the amount of reactivity inserted during a pulse.

An accumulator tank mounted on the core support carriage stores compressed air required to operate the pneumatic portion of the transient rod drive. A solenoid valve, located in the piping between the accumulator tank and the cylinder, acts as an on/off switch controlling whether or not air is supplied to the pneumatic cylinder. De-energizing the solenoid valve vents the compressed air supply and relieves the pressure in the cylinder, allowing the piston to drop by gravity to its lower limit, thereby fully inserting the transient rod into the core. This design ensures that the transient rod is fully inserted into the core except when compressed air is supplied to the cylinder and the anvil is raised above its lower limit.

The electromechanical portion of the transient rod drive consists of an electric motor, a ball-nut drive assembly, and the externally-threaded air cylinder. During electromechanical operation of the transient rod, the threaded section of the air cylinder acts as the screw in the ball-nut drive assembly. These threads engage a series of balls contained in the ball-nut drive assembly of the drive housing. The ball-nut assembly is then connected through a worm gear drive to an electric motor. Therefore, the cylinder and the anvil at its upper end may be raised or lowered independently of the piston and the transient control rod by using the electric drive when compressed air is not supplied to the cylinder. Conversely, when compressed air is supplied and the electromechanical drive is raised from its lower extreme, the transient rod operates like a standard control rod.

A system of microswitches is used to indicate the position of the air cylinder (anvil) and the transient rod. Two of these switches, the (anvil) DRIVE UP and (anvil) DRIVE DOWN microswitches, are actuated by a small bar attached to the bottom of the air cylinder. This bar extends through the rod support guide to prevent rotation of the cylinder. A third microswitch, the ROD DOWN microswitch, is actuated when the piston reaches its lower limit of travel. The transient rod anvil position, measured by a potentiometer on the drive motor, is displayed on the reactor console. If the reactivity worth of the total transient rod exceeds \$4.00, a mechanical stop is installed on the drive to prevent withdrawal of the piston past the Technical Specifications pulse limit of \$4.00. The mechanical stop may be removed for testing or calibration, but no pulses will be fired with the stop removed.

Figure 4-14 Transient Control Rod

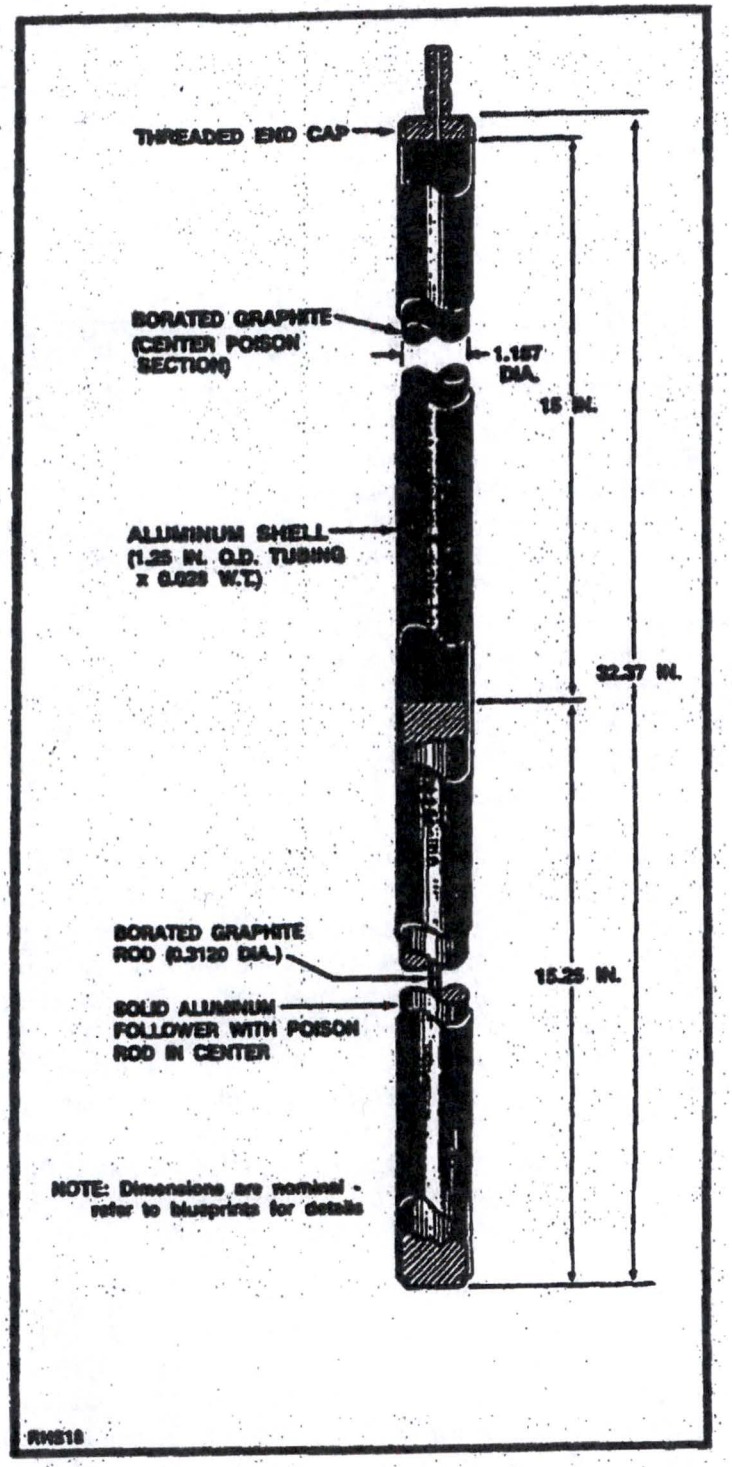

4.7 THERMAL-HYDRAULIC DESIGN

The thermal-hydraulic design of the AFRRI reactor is described in this section. The reactor is operated with natural convection cooling at all power levels and in all operational modes. For the purpose of this thermal hydraulic analysis, the term "rod" is used interchangeably with "element", so that "Average Rod", "Maximum Rod", and "Hot Rod" refer to thermal conditions in specific locations within the core structure.

4.7.1 Analysis of Steady State Operation

A thermal evaluation was made for the AFRRI reactor with a circular arrangement and operating with cooling from natural convection water flow through the core. The steady state thermal-hydraulic performance of the reactor was determined for operation at 1.1 MW and with a water inlet temperature of 48°C. This analysis provides the basis for the Technical Specification limit of 1.1 MW maximum operating power. Section 3.3 of the Technical Specifications states that the water temperature at the inlet to the purification system shall not exceed 60°C. The thermal analysis shows that a reactor inlet temperature of 48°C will yield a pool-core outlet mixed temperature of 60°C. Hence, the pool-core water inlet temperature is taken as 48°C.

The RELAP5 computer code (Reference 4-6) calculates the thermal hydraulics and fuel element temperatures in nuclear reactors. In this application, it is used to calculate the steady state natural convection flow through a vertical water coolant channel adjacent to a fuel element heat source. The code also calculates all radial thermal fluxes through the fuel element to the natural convection flow. Accordingly, the code determines the clad, fuel and Zr center rod temperatures within the fuel element and the axial temperature distribution of the natural convection flow.

The RELAP5 thermal analysis for the AFRRI-TRIGA reactor is based on a circular arrangement of fuel elements. The RELAP5 model contains two separate fuel rods (elements) and their corresponding flow channels. An "average rod" represents the average of the 88 fuel elements (85 from the standard fuel elements and 3 from FFCRs) in the entire core. A "maximum rod" represents the single hottest fuel element in the core. There is no communication in the code model between these two fuel rods and their flow channels, except that the static pressures of each flow are equal at the core inlet and core outlet. The AFRRI reactor has an aluminum adapter (shroud) which extends five feet from the core top grid plate. The diameter of the adapter equals the diameter of the core aluminum shroud. At the top of the adapter, the core outlet flow and pool water communicate again. The pressure of the core outlet flow equals the pressure of the cold water column outside of the core at this elevation. The core height plus the adapter height provide the buoyancy head for the core natural circulation.

The vertical flow channels within the circular core arrangement vary throughout the core. The "average rod" flow channel represents an average channel for those flow channels within the core. As such, a cross-sectional area is first calculated as the total core cross-sectional area to the outer radius of the F ring. The cross-sectional area of the total number of rods within this radius (91 rods) is then subtracted from the first area to obtain the total core flow area. Dividing this total area by the total number of rods yields the flow area per rod for the core "average rod".

The wetted perimeter and the heat source in the model equal the values for a single element multiplied by the number of fuel elements (88). In this manner, the RELAP5 output gives the total flow rate, the total power, and the average temperature for the heated core.

The tri-cusp area between the core center rod, A-1, and two adjacent B ring rods forms the minimum flow area in the core and includes the maximum power rod. The three rods that form this tri-cusp flow area constitute one-half of a rod. Additionally, the heated perimeter for this flow area represents only one-third of a rod because the central location A-1 is not a fuel rod. Customarily, this area is doubled to represent the flow area and hydraulic diameter for a whole rod. The flow area then represents two-thirds of a heated rod. Input to RELAP5 for the "maximum rod" is two-thirds of a rod surface area and two-thirds of the hot rod power.

The RELAP5 model of both the average and hot rods contains the heated fuel section and the unheated sections below and above the heated section. These latter sections represent the rod end reflectors and the rod end fittings. A single inlet flow loss coefficient represents the flow losses associated with the bottom grid plate and the bottom rod fittings. This inlet loss coefficient is estimated by first calculating the individual contraction and expansion losses from the pool to the beginning of the full diameter rod. The sum of these losses is then converted to the single inlet loss coefficient based on the rod flow area. A similar calculation is performed for the exit loss coefficient that represents the losses of the flow expansions and contractions from the top end of the full diameter rod, through the grid plate and into the adapter flow region. Details of this type of calculation are shown in GA-ESI, 2008 (Reference 4-7).

Figure 4-15 illustrates the RELAP5 model used for the AFRRI thermal-hydraulics analyses. The figure shows the separate average and maximum fuel rod heated sections ("heat structures") and associated flow channels ("pipes"). Branches represent the lower and upper unheated sections of the fuel rods. "Junctions" prior to the inlet of the lower branches and following the outlet of the upper branches provide the respective inlet and outlet flow losses. A flow volume ("pipe") above the core represents the core adapter shroud. The core average channel flow and hot channel flow thermally mix in this adapter "pipe". The two flow ("pipe") volumes parallel to the average, maximum and adapter flow channels model the cold water column adjacent to the core and adapter. A "pipe" above these components represents the water tank volume above the core. A time-dependent-volume ("tmdpvol") with an associated "junction" at the bottom of the diagram fixes the pool inlet flow rate and its temperature to the core and the flow volume adjacent to the core. Similarly, a "tmdpvol" at the top of the diagram fixes the ambient pressure above the pool, and serves as a flow sink for the reactor flows.

The RELAP5 model assumes that there is no cross-flow between the hot rod flow channel selected for analysis and other adjacent channels. (The average rod implicitly assumes that it is surrounded by similar rods.) A lateral pressure difference between the hot rod channel and an adjacent colder channel along the channels would provide a cross flow. Pressures at the core inlet and core outlet are equal for adjacent channels. Thus, there is likely little difference in pressure between two channels as one traverses from the bottom of the core to the top of the core. A small, if any, cross flow would be expected.

An examination of the overall buoyancy/friction pressure changes in channels adjacent to the hot channel indicates that the cross-flow would be from the cooler channel to the hot channel. The hot channel flow rate would increase. The hot channel density (buoyancy) would decrease (become colder) and diminish any cross-flow.

In a RELAP5 analysis of the McClellan Nuclear Radiation Center (MNRC) 2 MW reactor, Jensen and Newell (Reference 4-8) state the following: "The RELAP5 code provides a means for estimating the effects of cross-flow between the hot and average channels. The cross-flow effect is expected to be very small, and it is impossible to assess the accuracy of computed cross-flows. Scoping calculations with RELAP5 showed cross-flow to have no effect on fuel temperature and to increase slightly the critical heat flux ratio. Thus, cross-flow is conservatively neglected in this analysis."

These conclusions are supported in the recent STAT-RELAP5 comparison study, GA-ESI, 2008 (Reference 4-7). That study shows that fuel temperatures are little affected by the channel flow rate because the channel is in sub-cooled nucleate boiling. The bulk flow saturation pressure mostly determines the bulk flow temperature and subsequent fuel element temperatures.

There will be some change in the departure from nucleate boiling ratio (DNBR), also referred to as the critical heat flux ratio (CHFR), because there is a velocity (mass flux) effect in the DNB correlations. Calculations have shown that a 20% increase in the channel flow rate for a 1 MW reactor produces approximately a 2% increase in the wall heat flux (reactor power) to re-achieve a DNBR = 1.0.

As noted in the Sandia report by Rao, 1994 (Reference 4-9), various experiments have revealed that cross flow is negligible for tightly packed geometries such as the AFRRI-TRIGA reactor. The references for these experiments are Becker , 1969 (Reference 4-10), Silvestri, 1966 (Reference 4-11), and Gaspari, 1974 (Reference 4-12). The Sandia report further states that the ultimate effect of cross flow is to increase the DNBR, so that neglecting a sub-channel approach results in a conservative estimate of the DNBR.

The reactor power for predicting the critical heat flux (CHF), or departure from nucleate boiling (DNB), is calculated using the Bernath CHF correlation (Bernath, 1960 (Reference 4-13)). The Bernath correlation has historically been used for TRIGA reactor DNB predictions. In the current AFRRI DNB analysis, the RELAP5 code provides the thermal-hydraulic conditions needed for input to the Bernath correlation. A recent Groeneveld 2006 CHF correlation, (Groeneveld, 2007 (Reference 4-14)), also appears applicable for TRIGA DNB calculations. However, the Bernath correlation gives a lower (more conservative) DNB reactor power then the Groeneveld correlation. The Bernath correlation is used in this analysis.

4.7.2 RELAP5 Code Analysis

Input to the RELAP5 program includes the following:

1) Full geometry of the selected fuel elements and flow channel;
2) Radial and axial heat source distribution within the fuel;

3) Discretized axial spacing of the flow channel and the fuel element, and discretized radial spacing in the fuel element;
4) Pool height above the core;
5) Inlet and exit pressure loss coefficients;
6) Inlet water temperature.

The fuel element geometry and hydraulic data for the AFRRI RELAP5 model are given in Table 4-16.

Table 4-16 RELAP5 Input for Reactor and Core Geometry and Heat Transfer, AFRRI

Core and Reactor Geometry	
Unheated core length at inlet	(b)(7)(F)
Unheated core length at outlet	
Distance from top of pool surface to top of core	4.2672 m (14.0 ft)
Core adapter length	1.524 m (5.0 ft)
Core Hydraulic Data	
Inlet pressure loss coefficient	1.3
Exit pressure loss coefficient	0.3
Ambient pressure at pool surface	0.1014 MPa

As indicated in Section 4.7.1, the AFRRI RELAP5 thermal-hydraulic model contains an average element and its flow channel and a maximum powered element and its channel. Table 4-17 provides the RELAP5 hydraulic characteristics for these single elements and associated flow channel. The flow area and wetted perimeter for the average channel is the number of fuel elements (88) multiplied by the values in Table 4-17.

Table 4-17 Hydraulic Flow Parameters for a Single Element in an Element Cluster, AFRRI

Number of fuel elements	88
Fuel element heated length	(b)(7)(F)
Fuel element diameter	
Fuel element heated surface area (As previously noted, the RELAP5 hot element heated surface is 2/3's of a full element.)	
Average element:	
Flow area - average	5.3263 cm^2 (0.82558 in^2)
Wetted perimeter	11.770 cm (4.6338 in.)
Hydraulic diameter	1.8101 cm (0.71265 in.)
Hot element:	
Flow area - average	3.2076 cm^2 (0.49712 in^2)
Wetted perimeter	11.770 cm (4.6338 in.)
Heated perimeter (2/3 element)	7.8467 cm (3.0892 in.)
Hydraulic diameter	1.0901 cm (0.42917 in.)

The axial power distribution in the fuel section of the hot element is shown in Figure 4-16. The plot shows the axial power factor (apf), which is normalized to unity over the fuel section length. The hot element peak axial power factor is 1.343. The hot element power factor is 1.560 – the hot element power is 1.560 times the average element power. The average element peak axial power factor is 1.316. The radial profile of the power generated within the fuel region is shown in Figure 4-17. Figure 4-17 is a plot of the intra-element axial power factor. This factor is normalized to unity over the radial distance of the fuel region.

The heat generation in the fuel element is distributed axially over 25 uniformly spaced intervals to represent the curve in Figure 4-16. The heat generation in the fuel is distributed radially over 20 uniformly spaced intervals to represent the curve in Figure 4-17.

The heated length of the fuel element has the following radial dimensions:

Center zirconium rod diameter 0.635 cm (0.250 in.);
Fuel outer diameter (b)(7)(F) ;
Clad outer diameter cold (b)(7)(F) .

A fuel-to-clad gap is included in the RELAP5 model. This gap varies with the temperature of the fuel and the stainless steel cladding due to the relative thermal expansion between these two components at different reactor powers. Since the average core temperature of the average element and the maximum fuel temperature of the hot element are of interest, the gap widths differ for these two elements. Table 4-18 shows the average element and hot element radial gap widths used in the RELAP5 model.

Table 4-18 Fuel-to-Clad Radial Gap Widths for AFRRI RELAP5 model.

MW	Average Element	Hot Element
1.1	0.00635 mm (0.25 mils)	0.00254 mm (0.10 mils)

The above gaps were estimated from results of a recent RELAP5 analysis of the Puerto Rico Nuclear Center (PRNC) reactor.

Air at low pressure is assumed to fill the RELAP5 gap. As fuel burnup progresses, hydrogen or fission gasses may diffuse into the gap. These have either a higher thermal conductivity than air or they are in low concentration. As reactor operation continues, swelling of the fuel tends to decrease the gap width. A possible decrease in the gap gas thermal conductivity would be offset by the decreased gap width. A gas volume at the top of the fuel element essentially controls the pressure in the gap so no large drop in gap pressure would occur if induced by some means.

4.7.3 RELAP5 Code Results

Table 4-19 summarizes the thermal results for the AFRRI RELAP5 analysis for a 1.1 MW core. The table includes several RELAP5 input data for completeness.

Figure 4-18 shows axial temperature profiles for the core centerline, the clad mid-radius, and the bulk flow for the hot element. Figure 4-19 shows the fuel element radial temperature profile at the axial location of the maximum fuel temperature in the hot element. Both plots are for 1.1 MW.

The combination of RELAP5 thermal-hydraulics and the Bernath critical heat flux correlation was used to determine the maximum reactor power at which the departure of nucleate boiling, DNB, would occur. The reactor power for DNB is obtained using an inlet temperature of 48°C. Then the reactor power is systematically increased until a local wall heat flux in the hot element equals the DNB flux as predicted by the Bernath correlation. At this power, the ratio of the predicted DNB flux divided by the wall heat flux equals 1.0. The maximum AFRRI reactor power for which this ratio equals unity is 1.99 MW. The corresponding hot element power is 35.3 kW/element.

Table 4-19 AFRRI TRIGA Thermal Results Summary for a 1.1 MW Core

Parameter	Initial Core
Axial peaking factor – average element	1.316
Axial peaking factor – hot element	1.343
Hot element power factor	1.560
Inlet coolant temperature	48°C, 118°F
Coolant saturation temperature at core inlet	110.3°C, 230.5°F
Exit coolant temperature – average element	67.11°C, 152.8°F
Exit coolant temperature – hot element	82.51°C, 180.5°F
Average temperature in pool above core	60.2°C, 140.4°F
Coolant mass flow	13.60 kg/sec, 107,900 lb/hr
Average flow velocity	29.48 cm/sec, 0.967 ft/sec
Core average fuel temperature	247.1°C, 476.7°F
Peak fuel temperature in average fuel element	360.0°C, 679.9°F
Maximum wall temperature in hot element	149.2°C, 300.6°F
Peak fuel temperature in hot fuel element	440.7°C, 825.3°F
Average heat flux	27.87 W/cm^2, 88,362 $BTU/hr\text{-}ft^2$
Maximum heat flux in hot element	58.40 W/cm^2, 185,125 $BTU/hr\text{-}ft^2$
Minimum DNB ratio at 1.0 MW	1.99

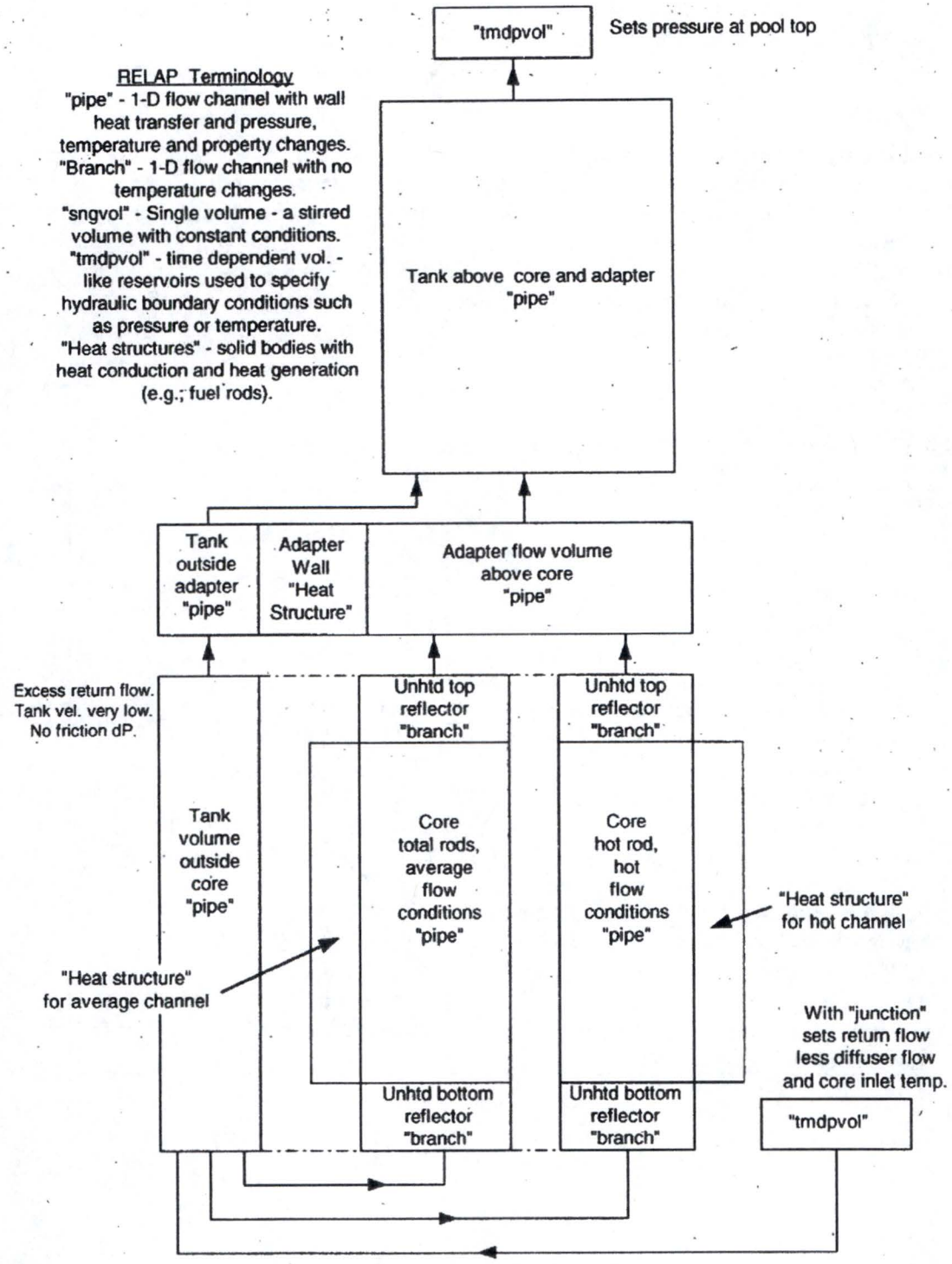

Figure 4-15 AFRRI RELAP5 Block Diagram

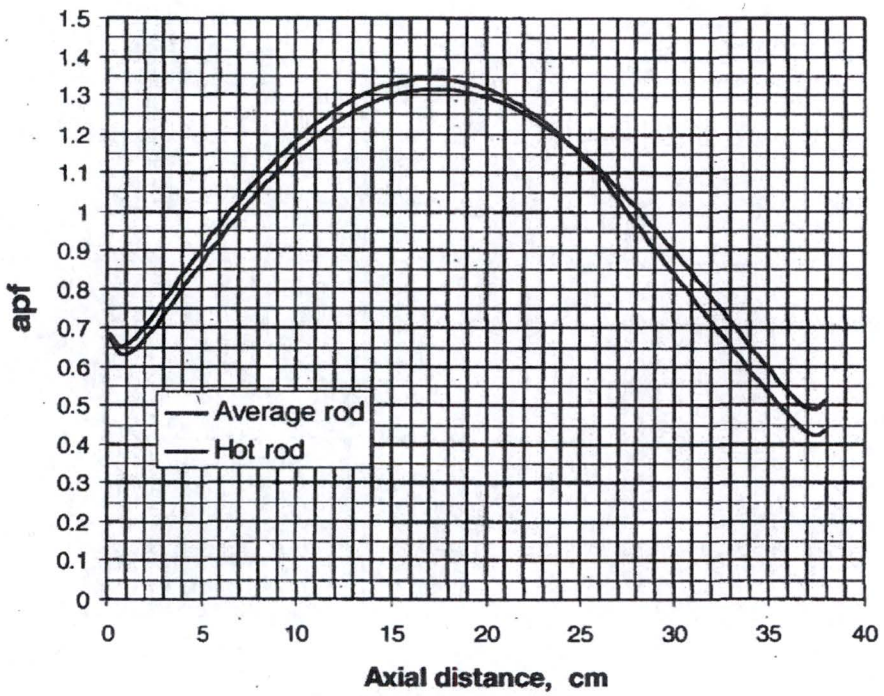

Figure 4-16 AFRRI Axial Power Factor versus Fuel Element Heated Length

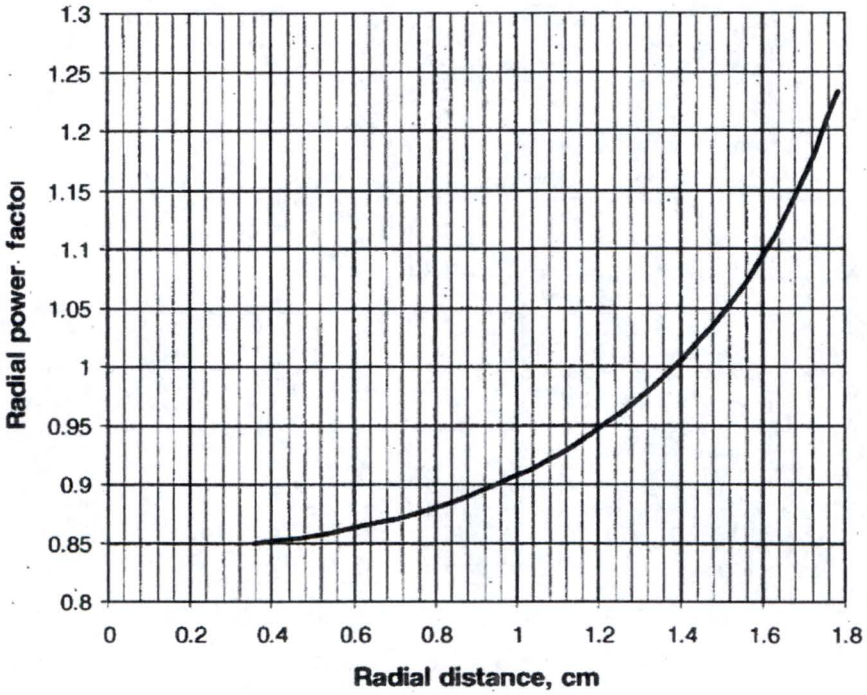

Figure 4-17 AFRRI Radial Intra-Element Power Factor versus Fuel Element Radial Distance

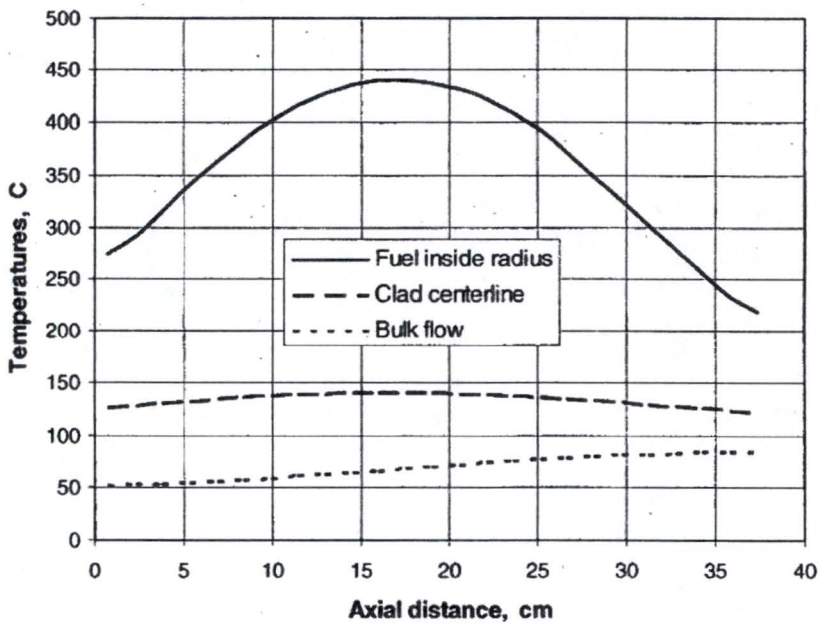

Figure 4-18 AFRRI Temperature Axial Profiles

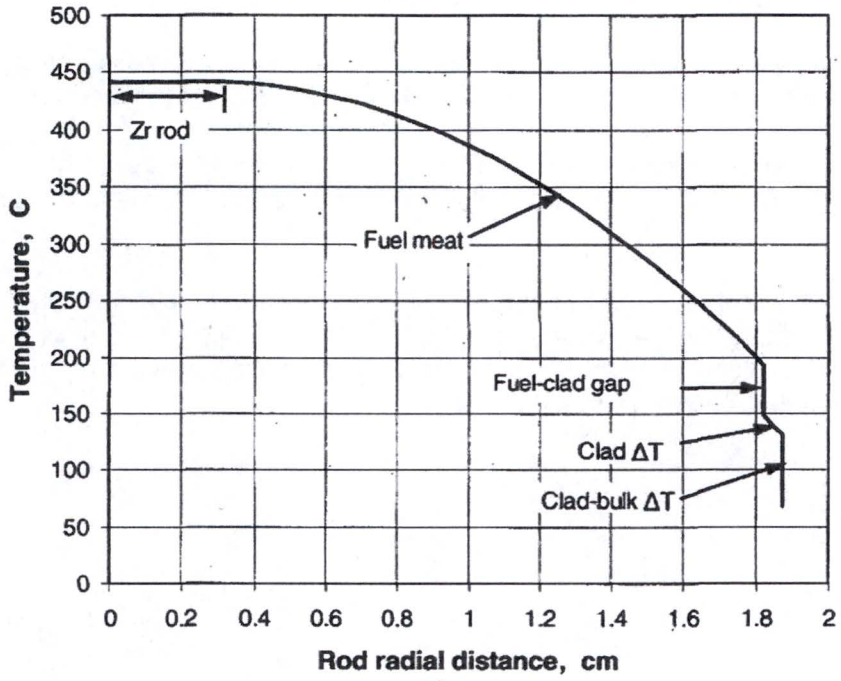

Figure 4-19 AFRRI Temperature Radial Profile

4.9 THERMAL NEUTRON FLUX OF THE 85-3 CORE AT BOL

The thermal neutron fluxes (E < 0.42 eV) were calculated with the DIF3D code using the R-θ-Z, 3D model of the AFRRI 85-3 core at 280°C, BOL and with all control rods withdrawn.

Figure 4-20 shows the plane view of the core with the 85 fuel elements, 3 FFCRs, 1 transient control rod, Al tube-filled (E-23) hole, and water-filled (F-9) hole with the azimuthal angle (θ) direction.

The calculated maximum thermal neutron flux at the axial centerline of the fuel elements is 2.454×10^{13} (n/cm^2-sec) in the A-1 location, at r =1.697 cm, θ = 172 degrees. Figures 4-21 through 4-24 show the thermal neutron fluxes for the 85-3 core at the axial centerline of the fuel element for 90 degrees azimuthal angle increments.

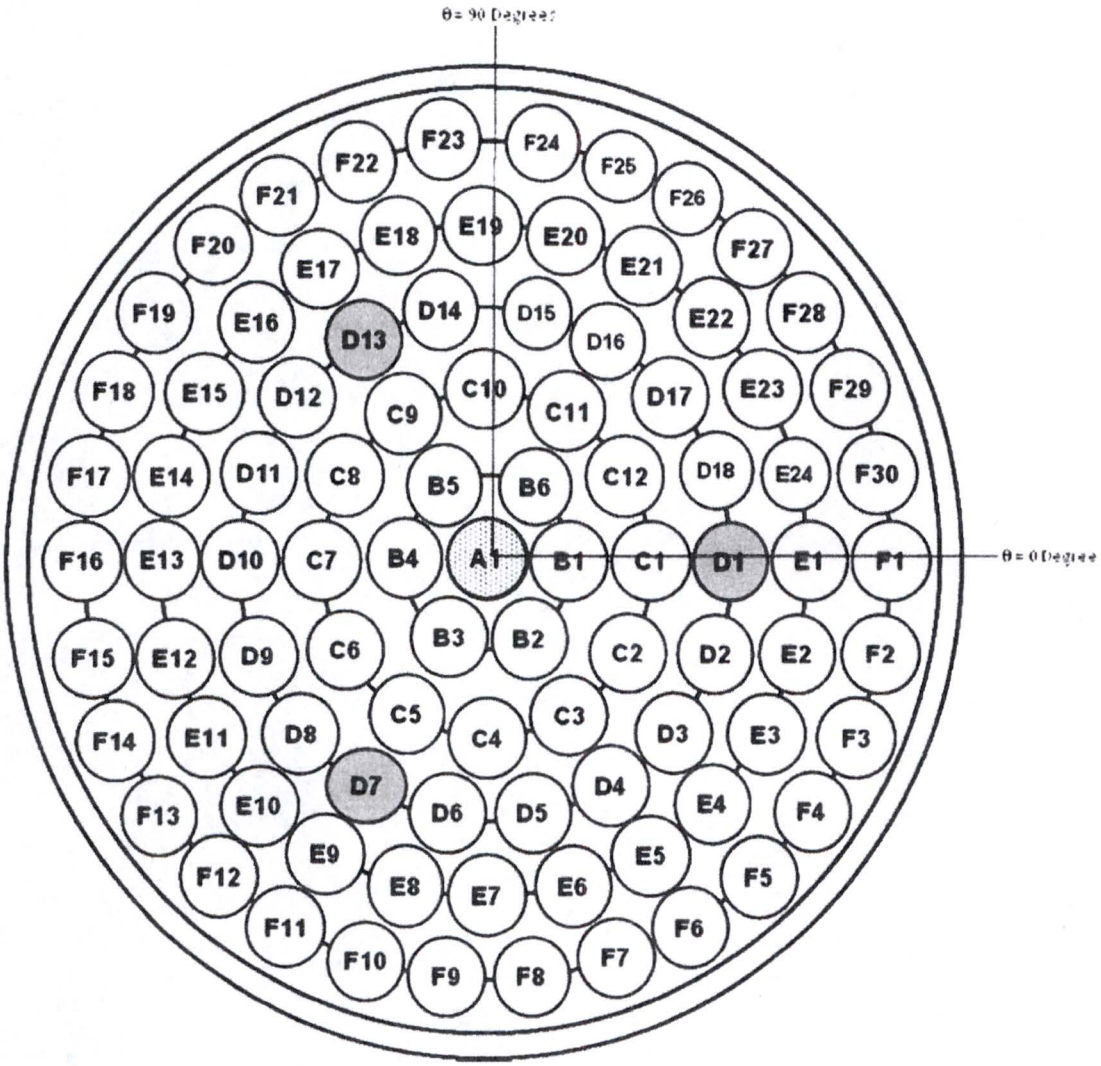

Figure 4-20 The Plan View of the 85-3 AFRRI Core

D-1, D-7, D-13:	FFCRs
A-1:	Transient Control Rod
E-23:	Non-Fuel Location, Al Tube-Filled Hole
F-9:	Non-Fuel Location, Water-Filled Hole

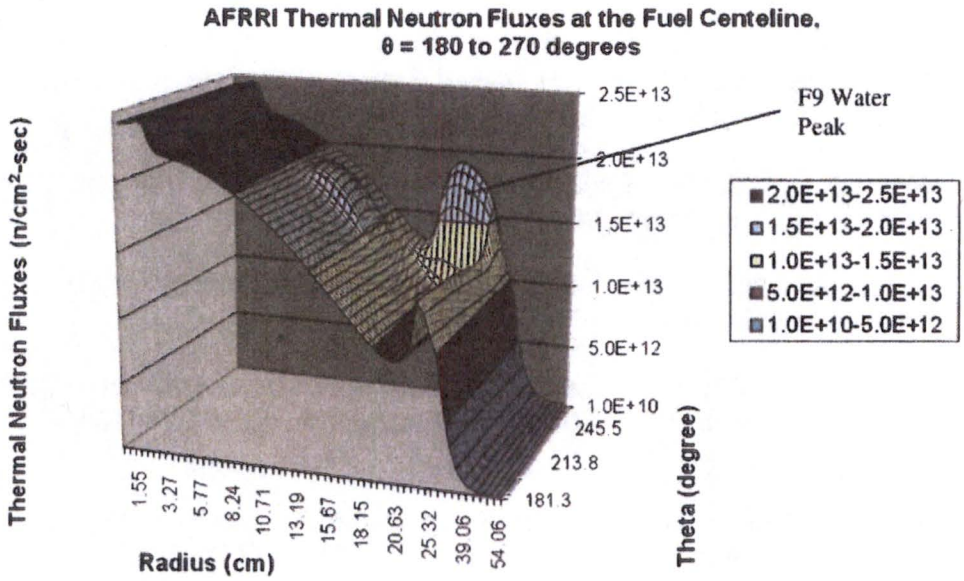

Figure 4-23 Thermal Neutron Fluxes (n/cm^2-sec) (E < 0.42 eV) at the fuel axial centerline, for the 85-3 AFRRI Core at BOL, 280°C, θ = 180 to 270 degrees

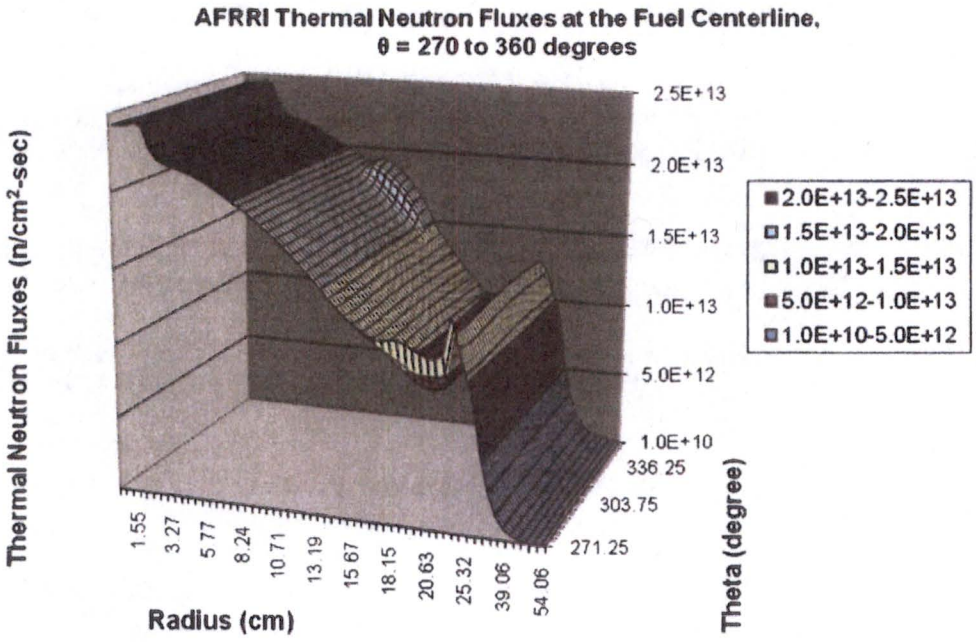

Figure 4-24 Thermal Neutron Fluxes (n/cm^2-sec) (E < 0.42 eV) at the fuel axial centerline, for the 85-3 AFRRI Core at BOL, 280°C, θ = 270 to 360 degrees

References

4-1 Lawrence, R.D., "The DIF3D Nodal Neutronics Option for Two-and-Three-Dimensional Diffusion Theory Calculations in Hexagonal Geometry," Doc. No. ANL-83-1, Argonne National Laboratory, March 1983.

4-2 Derstine, K.L., "DIF3D: A Code to Solve One-, Two-, and Three-Dimensional Finite Difference Diffusion Theory Problems," Doc. No. ANL-82-64.

4-3 Los Alamos MCNPX Team, "MCNPX – A General Monte Carlo N-Particle Transport Code, Version 2.6.0," LA-CP-07-1473, April 2008.

4-4 R. Sherman, "BURP: A Macroscopic Cross Section Generation and Nuclide Depletion Program for Use with DIF3D", General Atomics report CEGA-M-93-1139, August 1993.

4-5 Mathews, D.R., et. al., "GGC-5, A Computer Program for Calculating Neutron Spectra and Group Constants," Gulf General Atomic Report GA-8871, 1971.

4-6 INEL, (1995), RELAP5/Mod 3 Code Manual, Vol. 1-5, Idaho National Engineering Laboratory, NUREG/CR-5535.

4-7 GA-ESI, (2008), TRIGA Reactor Thermal-Hydraulic Study, TRD 070-01006.04, Rev. A, Prepared by TRIGA Reactors Division of General Atomics-ESI, April 2008.

4-8 Jensen, R. T., and D. L. Newell, (1988), "Thermal Hydraulic Calculations to Support Increase in Operating Power in McClellan Nuclear Radiation Center (MNRC) TRIGA Reactor," 1998 RELAP5 International User's Seminar, College Station, Texas, May 1998.

4-9 Rao, D. V., and M. S. El-Genk, (1994), "Critical Heat Flux Predictions for the Sandia Annular Core Research Reactor," Sandia report SAND 90-7089, August 1994.

4-10 Becker, K. M., G. Hernborn, M. Brodl, and G. Erikson, (1969), "Burnout Data for Flow of Boiling Water in Vertical Round Ducts, Annuli and Rod Clusters, AE-177, AB Atomenergi, Sweden, 1969.

4-11 Silvestri, M., (1966), "On the Burnout Equation and on the Location of Burnout Points," Energia Nucleare, Vol. 13, No. 9, pp. 469-479, 1966.

4-12 Gaspari, G. P., A. Hassid, and F. Lucchini, (1974), "A Rod Centered Subchannel Analysis with Turbulent Mixing for Critical Heat Flux Prediction in Rod Clusters Cooled by Boiling Water," Paper B6.12, Proc. Fifth Int. Heat Transfer Conf., 1974.

4-13 Bernath, L., (1960), "A Theory of Local Boiling Burnout and Its Application to Existing Data," Heat Transfer-Chemical Engineering Progress Symposium Series, Sorrs, Connecticut, v. 56, No. 20, 1960.

4-14 Groeneveld, D.C., et al, (2007), "The 2006 CHF Look-up Table," *Nuclear Engineering and Design*, Vol. 237, 2007, pp. 1909-1922.

13 ACCIDENT ANALYSES

In this chapter of the SAR, information and analyses are presented that show that the health and safety of the public and workers are protected. Potential radiological consequences in the event of malfunctions are presented, along with the capability of the facility to accommodate such disturbances. The accidents analyzed range from anticipated events to a postulated fission product release with radiological consequences that exceed those of any accident considered to be credible. This limiting accident is referred to as the maximum hypothetical accident (MHA).

13.1 ACCIDENT-INITIATING EVENTS AND SCENARIOS

This section of the SAR describes potential accident-initiating events and scenarios for the AFRRI-TRIGA Mark-F reactor.

Nonroutine operational risks may arise from the improper handling of radioactive material or from malfunctions of materials and equipment. The specific malfunctions investigated are loss of cooling water, radioactive contamination of the reactor pool water, and fuel element cladding failure. The consequences of the nonroutine operational risks are specifically addressed in Section 13.2.

Routine operational risks are present in the manipulation of any radioactive material because of the potential for biological and physical damage. The following sections investigate potential consequences associated with routine operation, including the handling of radioactive materials, reactor power transients, experiments associated with reactor operations, and production of radioactive gases (primarily through activation of argon).

13.1.1 Handling Radioactive Material

Because of the potentially harmful biological effects of radioactive material, precautions are taken in the handling of these materials. Reactor operations must be supervised by responsible individuals who are trained in the detection and evaluation of radiological consequences. Administrative, operational, and health physics procedures will be followed, and special equipment and procedures which are needed to maintain the "as low as reasonably achievable" (ALARA) concept of radiation protection will be used.

The radiological consequences associated with fuel elements are of the same nature as those associated with isotope production. Because of their high radiation levels, irradiated fuel elements are kept underwater for shielding purposes. In keeping with ALARA policies, a fuel element would generally not be removed from the reactor pool for at least two weeks following its use in the reactor core. When a fuel element is removed from the reactor tank, a conventional fuel element transfer cask may be used to reduce radiation levels to within acceptable limits. The nonroutine event of dropping a fuel element during such a transfer which results in a cladding failure in air is addressed in Section 13.2.4.

When proper administrative, operational and health physics procedures are utilized, the handling of radioactive materials does not represent a significant risk to the health and safety of operating personnel or the general public.

13.1.2 Reactor Power Transients

The following discussion is based on experiments and tests performed by General Atomics (GA, 1980, Reference 13-1 and Simnad, 1976, Reference 13-2). Theoretical estimates are also reviewed. The U-ZrH fuel elements used in the TRIGA reactor are capable of operating under conditions of transient experiments for delivery of high intensity bursts of neutrons. Fuel elements with 8.45 wt% U have been pulsed repeatedly in General Atomics' Advanced TRIGA Prototype Reactor (ATPR) to peak power levels of over 8,000 MW providing a neutron fluence per pulse of approximately 1.0×10^{15} nvt (neutrons/cm^2).

The ATPR fuel elements were subjected to thousands of pulses of 2,000 MW or more. The inherent safety of the fuel element stems from its large prompt negative temperature coefficient of reactivity, which causes the automatic termination of a power excursion before any core damage results. This temperature coefficient has been measured to be approximately \$0.018 reactivity loss per 1°C rise in fuel temperature, i.e., -1.26×10^{-4} $\Delta k/k/°C$.

The reactor loading is limited by the Technical Specifications to a maximum of 3.5% $\Delta k/k$ (\$5.00) excess reactivity above cold critical, with or without all experiments in place. Thus, the maximum reactivity transient that could possibly occur would be that produced by the rapid insertion of the entire available amount of excess reactivity. In regard to TRIGA fuel performance, experiments at General Atomics' ATPR have been performed for step insertions of up to 3.5% $\Delta k/k$ (\$5.00) reactivity. The fuel elements were subjected to thousands of pulses of 2,000 MW or more and attained temperatures of up to 1,000°C. For example, the annular core TRIGA reactor at JAERI (Japan) has operated since 1975, with over 1,000 pulses of all sizes at fuel temperatures up to 1,000°C. From the results of the tests performed by General Atomics, there was no external evidence of change in any of the five special test elements in the first 200 pulses.

Theoretical estimates based on the Fuchs-Nordheim mathematical model of the AFRRI-TRIGA reactor have also been made. These calculations indicate that a step insertion of 2.8% $\Delta k/k$ (\$4.00 when $\beta_{eff} = 0.07$) (AFRRI-TRIGA Technical Specification limit) would result in a fuel temperature rise of less than 550°C.

Therefore, based on operating experience of the ATPR and the Fuchs-Nordheim mathematical model, it can be concluded that the rapid insertion of the total authorized excess reactivity of 3.5% $\Delta k/k$ (\$5.00) would not represent an undue risk to the operating personnel or the general public.

13.1.3 Improper Fuel Loading

Fuel loading of the reactor is always supervised by trained, licensed supervisory personnel. All reactor monitoring and shutdown devices will be operational during loading. The worst possible

case of improper fuel loading would be for an operator to mistakenly insert a fuel element in a core that is already critical at a low power level, i.e., ≤1.0 W(t). In a core near its critical point, all of the inner fuel positions would be occupied so that the extra fuel elements could be added only in a peripheral position, where a fuel element worth is approximately 0.21% Δk/k ($0.30). Since step additions of 2.1% Δk/k ($3.00) excess reactivity are made on a routine basis for pulsing the reactor, the addition of 0.21% Δk/k ($0.30) would not present a danger of damaging the reactor or fuel. The reactor would undergo a mild transient and then operate at a steady-state power level of about 50 kW.

Even in the extremely unlikely event that a fuel element in the B ring should be improperly handled, its rapid insertion would result in an addition of about 0.67% Δk/k ($0.95). As indicated above, such an addition would not result in any damage to the reactor or the fuel and would not represent an undue risk to the health and safety of the operating personnel or the general public.

13.1.4 Production of Radioactive Gases in the Reactor Coolant

The production of radioactive gases by the reactor in its associated facilities originates through neutron activation of elements in the air or water. One of the most important of these activation products is radioactive argon (Ar^{41}), with a half-life of 1.83 hours. Calculations are based on a temperature of 70°F (21°C) and Ar^{40} content of air of 0.94 percent by volume.

In the calculation to determine the amount of argon dissolved in the reactor pool water, it is assumed that the argon follows Henry's Law. At a water temperature of 70°F (21°C), the corresponding water vapor pressure is 19 mm Hg. The partial pressure for air would therefore be 760 – 19 = 741 mm Hg. Using an argon content of air as 0.94 percent by volume, the resulting partial pressure of argon is 7 mm Hg. Applying Henry's Law, a saturation concentration of argon in water of 1.367×10^{-8} gm-mole/cm^3 water is obtained. Using a microscopic thermal neutron absorption cross section of 0.61×10^{-24} cm^2 for Ar^{40}, the macroscopic absorption cross section of argon in water becomes 5×10^{-9} cm^{-1}.

Activity production, assuming an Ar^{41} saturation condition has been achieved, can be calculated as:

$$A_p = \frac{\phi_n \left(1 - e^{-\lambda t_p}\right) \Sigma_a}{3.7 \times 10^4} \qquad (1)$$

where:

A_p	=	activity in reactor water (μCi/cm^3)
ϕ_n	=	thermal neutron flux (n/cm^2-sec)
t_p	=	core circulation time (sec)
Σ_a	=	macroscopic absorption cross section (cm^{-1})
λ	=	decay constant (sec^{-1})

A conservative value for the average thermal neutron flux (ϕ_n) in the reactor core is estimated to be 1.0×10^{13} n/cm^2-sec at a 1.0 MW power level. The water circulates through the core by

natural convection and is estimated to change completely in approximately 4 seconds. The Ar^{41} decay constant is 1.05×10^{-4} sec^{-1}. The core of the reactor holds 3.4×10^{4} cm^3 of water and the water flow rate through the core is 0.9×10^{4} cm^3/sec. Substituting the appropriate values in the above equation yields an Ar^{41} activity in the reactor water of:

$$A_p = \boxed{\text{(b)(7)(F)}}\ \mu Ci/cm^3,$$

and a total Ar^{41} production rate in the core of:

(b)(7)(F) $Q = \boxed{\quad}\ \mu Ci/sec.$

The travel time of Ar^{41} from the core to the water surface, a minimum distance of 457.2 cm (15 ft), has been estimated to be 24 seconds. Assuming the decay to be negligible, the maximum rate of activity reaching the surface is 5.1 μCi/sec.

(b)(7)(F) Under saturated, steady-state conditions, the maximum rate at which Ar^{41} can escape from the water surface will be $\boxed{\quad}$ μCi/sec, and an equivalent amount of Ar^{40} will dissolve into the water to replace the Ar^{41} depletion. As water temperature increases, the water vapor pressure will increase and the amount of dissolved Ar^{40} will decrease, resulting in a decreased generation of Ar^{41} escaping to the reactor room. The radioactive Ar^{41} will escape from the reactor pool, dissipate in the reactor room air, and circulate through the ventilation system. Estimates are that the reactor room exhausts 9.64×10^{7} cm^3/min (3404 ft^3/min) of the total 8.78×10^{8} cm^3/min (31,000 ft^3/min) through the AFRRI stack. The total exhaust value includes the reactor room exhaust, other radiological control areas, as well as non-radiation areas.

Since the air is exhausted from the system at a high rate, it is assumed that the Ar^{41} decay is negligible. If it is assumed that there is continuous reactor operating time, equilibrium conditions can be assumed. Since equilibrium conditions are assumed, the same concentration of Ar^{41} will exist in the reactor room as in the exhaust air. The concentration in the reactor room is:

$$\frac{\boxed{\text{(b)(7)(F)}}\ \mu Ci/\text{sec}}{\boxed{\text{(b)(7)(F)}}\ cm^3/\text{sec}} = \boxed{\text{(b)(7)(F)}}\ \mu Ci/cm^3$$

The concentration in the stack is $\boxed{\text{(b)(7)(F)}}$ μCi/cm^3 and is further dispersed in the atmosphere before reaching the surrounding population. The gamma dose rate in the reactor room can be estimated for the Ar^{41} concentration of $\boxed{\text{(b)(7)(F)}}$ μCi/cm^3 by assuming submersion in a spherical source equivalent to the reactor room volume. The dose equivalent rate can be given as:

$$D = \frac{S_\gamma}{K\mu}\left(1 - e^{-\mu r}\right) \qquad (2)$$

where:
- D = dose rate (rem/hr)
- S_γ = gamma source strength (MeV/cm^3-sec)
- μ = linear attenuation coefficient for air (cm^{-1})
- K = flux-to-dose conversion factor (MeV/cm^2-sec per rem/hr)
- r = radius of equivalent sphere (cm).

The volume of the reactor room is approximately 9.2×10^8 cm^3, which is equivalent to a sphere with a radius of 603 cm. An Ar^{41} concentration of (b)(7)(F) $\mu Ci/cm^3$ has a gamma source strength equal to 0.15 MeV/cm^3-sec (E_γ = 1.293 MeV/disintegration). For the Ar^{41} gamma photon of 1.293 MeV, the linear attenuation coefficient for air is 6.87×10^{-5} cm^{-1} and the flux-to-dose conversion factor is 5.86×10^5 MeV/cm^2-sec per rem/hr. Substituting these values into the above equation results in a dose equivalent rate of 0.15 mrem/hr. The yearly dose equivalent becomes 300 mrem for continuous exposure over a 2000-hour year, and it is more than an order of magnitude below the yearly occupational dose limit of 5 rem total effective dose equivalent (TEDE).

Another important activation product is radioactive nitrogen (N^{16}), with a half-life of 7.13 seconds. As a result of its short half-life, N^{16} contributes to the occupational dose of individuals in the reactor room during operation, particularly high power operations, but poses no danger to the health and safety of the general public. The activation occurs as a result of the oxygen content in the pool water from the $O^{16}(n,p)N^{16}$ production process which is exclusively a fast neutron (i.e., $\geq$0.1 MeV) induced activation reaction.

Since N^{16} is produced by fast neutron activation of oxygen in the pool water within the core region, the activity production and dose rate equations cited above were used to calculate radioactive nitrogen (N^{16}) releases from the reactor pool to the reactor room air, and the associated dose rates that conservatively would be expected above the pool water surface directly over the core.

The concentration of O^{16} in water is approximately 0.0554 gm-mole/ml of H_2O. Using a microscopic (n,p) cross section for O^{16} of 1.9×10^{-29} cm^2 which is averaged over the fission spectrum, the macroscopic (n,p) cross section for O^{16} in water becomes 6.34×10^{-7} cm^{-1}.

Using a conservative average fast flux value for the AFRRI-TRIGA reactor at 1.0 MW(t) of 5.0×10^{12} neutrons/cm^2/sec, and substituting the appropriate values for λ, t_p, Σ_a (i.e., $\Sigma_{n,p}$ for O^{16}) yields:

$$A_p = \text{(b)(7)(F)}\ \mu Ci/cm^3,$$

and a total N^{16} production rate in the core at 1.0 MW(t) of:

$$Q = \text{(b)(7)(F)}\ Ci/sec.$$

Using a measured travel time for N^{16} bubbles to rise from the core to the water surface of 24 seconds, the maximum rate at which activity from N^{16} reaches the pool surface is (b)(7)(F) Ci/sec.

The radioactive nitrogen will escape from the reactor pool, dissipate, and decay rapidly (7.13 second half-life) in the reactor room air. The volume of air above the surface of the reactor pool in which the N^{16} activity per second is distributed was assumed to be a right circular cylinder with a diameter of 91.5 cm and height of 100 cm for negligible decay. This assumed volume, therefore, is 6.58×10^5 cm^3. The concentration of N^{16} in this volume per second would therefore be (b)(7)(F) $\mu Ci/cm^3$ with a gamma source strength equal to (b)(7)(F) MeV/cm^3/sec (E_γ = 4.6

MeV/disintegration). For the N^{16} primary gamma photon of 6.13 MeV, the linear attenuation coefficient for air is 3.05×10^{-5} cm^{-1} and the flux-to-dose conversion factor is 9.62×10^{5} $MeV/cm^2/sec$ per rem/hr. Substituting these values into the appropriate equation using an equivalent volume sphere having a radius of 54 cm results in a conservative estimate of the dose rate due to N^{16} at 1.0 MW(t) of 350 mrem/hr immediately above the pool water surface directly over the core. It should be noted that the N^{16} activity evaluated by this analysis is due only to the amount of N^{16} that may be released from the pool. It should also be noted that due to the short half-life of N^{16} and the amount of time required to circulate air from the reactor room to the top of the AFRRI stack, essentially no N^{16} is released from the AFRRI stack to the environment. As a result, N^{16} only presents an occupational dose hazard to individuals in the reactor room near the pool surface during high power operation.

Based upon actual measurements made during reactor operations at 1.0 MW(t), the typical Ar^{41} release rate from the pool surface has been approximately [redacted] µCi/sec. Comparing this to the (b)(7)(F) calculated value of [redacted] µCi/sec indicates a factor of ten conservatism in the calculation. A typical Ar^{41} concentration at the top of the AFRRI stack has been approximately [redacted] µCi/cm^3 as compared to the calculated value of [redacted] µCi/cm^3, also indicating a factor of ten conservatism in the calculation.

Gamma radiation levels measured directly over the core just above the pool surface range from 75 mrem/hr initially to a maximum of about 200 mrem/hr. Gamma radiation levels measured around the reactor pool boundary chain range up to 14 mrem/hr. It should be noted that all measured gamma dose rates include N^{16} in both the pool water and the reactor room air. Even though the calculated dose rate for N^{16} of 350 mrem/hr only takes into account N^{16} in the reactor room air just above the pool surface, it still overestimates the actual dose rate by a factor of 1.5 during 1.0 MW operation.

13.1.5 Experiments

All experiments performed as part of the TRIGA reactor operations are reviewed by the Reactor and Radiation Facilities Safety Subcommittee and must be authorized prior to being conducted. The Technical Specifications contain requirements that must be met before such experiments can be performed using the AFRRI-TRIGA reactor. Experiments are always supervised by trained, licensed supervisory personnel. However, failure of an experiment is possible and worst-case conditions can be calculated to determine the postulated consequences.

The two worst-case conditions for failure of an experiment could result in instantaneous insertion of reactivity or the release of radioactive material from an experiment undergoing activation in the reactor. For an experiment failure in which reactivity could be added, the worst possible case would be the prompt addition of less than 0.36% Δk/k ($0.51) in either Exposure Room #1 or #2. As discussed for the case of improper fuel loading (Section 13.1.3), the addition of 0.36% Δk/k ($0.51) would be within the range of an improper fuel loading condition. Such an addition would not result in any damage to the reactor or the fuel. For an experiment failure in which radioactive material could be released from the experiment, i.e., activation products, the worst case would be the prompt release of the radioactive material to the atmosphere. An authorized experiment involves the irradiation of 20 liters of argon gas for one hour at a power level of 1.0

MW. The resulting activation would result in a total Ar^{41} activity of [redacted] Ci in the sealed container. If the container should fail and release all of the Ar^{41} activity, the resulting total whole body dose would be less than 2.7 mrem to an individual more than 35 meters from the AFRRI stack (Equation 9 in Section 13.2.3.3). The failure of this authorized experiment represents the worst case for radiological consequences from an experiment failure in the AFRRI-TRIGA reactor. Such a whole body dose would not represent an undue risk to the health and safety of the general public. (b)(7)(F)

13.2 ACCIDENT ANALYSIS AND DETERMINATION OF CONSEQUENCES

In order to evaluate the potential consequences associated with operation of this reactor the following assumptions have been made:

- The reactor will normally have two modes of operation:

  Steady-state operation at power levels not to exceed 1.1 MW for testing/maintenance purposes and 1.0 MW for normal operations. For calculations, the assumption of operation in the steady-state mode at a power level of 1.0 MW was utilized. The total reactor power generated has been approximately 1000 MW-hrs from June 1964 through 2009.

  Pulse operation achieved by intentionally placing the reactor on a prompt critical excursion by making a step insertion of positive reactivity above critical by utilizing the transient rod with appropriate scrams and interlocks. The maximum step insertion is limited by the Technical Specifications to 2.8% $\Delta k/k$ ($4.00) reactivity in the pulse mode. The average "maximum-pulse" used during AFRRI's TRIGA pulse operation has been 28 MW-sec. For calculations, the assumption of a maximum excursion pulse of 40 MW-sec was utilized as an upper limit for pulse operations or an inadvertent transient.

- The reactor operations will be supervised by individuals who are qualified operators trained in the detection and evaluation of radiological consequences.

13.2.1 Loss of Coolant Accident

A loss-of-coolant accident (LOCA) occurs when there is a leak in the reactor tank and the pool water drains to a level below the core. A shutdown scram is initiated before the water level falls to less than 14 feet above the core. The reactor power drops almost immediately to approximately 6 – 7% of normal power, and then continues to decay essentially exponentially. Core cooling is now dependent on ambient air natural convection through the core. A buoyancy force to drive this natural convection is developed by a hot air column within the core and a cooler air column outside of the core.

Typically, in LOCA analyses the air natural convection cooling is assumed to occur either at the time of scram (no delay) or 15 minutes after scram (15 minute delay). The zero start time assumes the water drains immediately and that there is no delay in the decay power level. A 15 minute delay assumes that the water drains at a reasonable, finite rate and maintains some

cooling of the core during this drain time. The core becomes completely uncovered after 15 minutes, and the air natural convection cooling and decay heat start at this delayed time. Two different decay heat versus time curves are also specified based on the amount of full power operation – data source (ANS, 2005, Reference 13-3) - an "infinite" reactor irradiation time (10^{13} seconds – over 300,000 years) or a "72 hour" reactor irradiation. This model assumes 72 hours of operation per week for a period of 40 years. Data for these two decay curves are presented in Table 13-1.

13.2.1.1 TAC2D Computer Program

The TAC2D computer code, along with user-supplied equations to calculate the air natural convection, is used to model the AFRRI LOCA event. TAC2D is a transient, two-dimensional thermal conduction code developed by General Atomics (GA, 1976, Reference 13-4). In addition to conduction, the code allows for radiation among solid surfaces, and for the heating or cooling of fluid flows parallel to solid surfaces. The code is written in FORTRAN and selected subroutines are compiled to provide an executable version. A FORTRAN subroutine called "prop.for" is supplied for the user to input thermal properties. Properties may be described by any type of FORTRAN routine. Via this "prop.for" subroutine, the user may provide temperature dependent properties, radial and axial fuel power distributions, and wall to fluid heat transfer correlations. Time dependent functions, such as a reactor decay heat curve, may also be provided. The "prop.for" subroutine is compiled and linked upon code execution. The code accepts user-supplied subroutines, where the user may write programming to describe other physical phenomena associated with the analysis at hand. Such a subroutine was constructed for the AFRRI LOCA analysis to compute the time-dependent natural convection cooling air flow through the AFRRI core. Any such subroutines are also compiled and linked upon execution.

The TAC2D code includes defining multiple one-directional flow channels parallel to solid surfaces with heat exchange between the surface and the channel flow. Fluid properties and wall-to-flow heat transfer correlations are input to the "prop.for" subroutine. However, the channel flow rate must be defined by the user. A user-defined subroutine can be used to calculate a thermally-driven and time-dependent flow rate.

The geometry of a thermal model is provided by an input file read by TAC2D upon execution.

13.2.1.2 TAC2D LOCA Thermal Model

The TAC2D model for the LOCA event is a two-dimensional, radial-axial geometry. The model contains one fuel element and its associated flow channel representing the core hot rod. The model includes the fuel and zirconium rod, bottom and top graphite reflectors and end fixtures, the void between the top graphite and top end fixture, and the rod clad. Figure 13-1 shows the TAC2D model geometry.

Table 13-1 ANSI/ANS-5.1-2005 Decay Heat Standards

Infinite (10^{13} s) Operation Time and
Operation for 72 Hours/Week for 40 Years.

t (sec)	72 Hours/week (for 40 years)	*Infinite Operation (10^{13} sec)*
0	6.473%	
1	5.937%	*6.190%*
1.5	5.752%	*6.005%*
2	5.600%	*5.850%*
4	5.167%	*5.420%*
6	4.880%	*5.130%*
8	4.665%	*4.917%*
10	4.497%	*4.749%*
15	4.192%	*4.443%*
20	3.979%	*4.230%*
40	3.480%	*3.732%*
60	3.195%	*3.446%*
80	2.997%	*3.249%*
100	2.850%	*3.101%*
150	2.599%	*2.850%*
200	2.435%	*2.687%*
400	2.084%	*2.336%*
600	1.892%	*2.144%*
800	1.755%	*2.007%*
1000	1.649%	*1.900%*
1500	1.455%	*1.706%*
2000	1.319%	*1.570%*
4000	1.019%	*1.269%*
6000	0.869%	*1.119%*
8000	0.775%	*1.024%*
10000	0.707%	*0.956%*
15000	0.596%	*0.844%*
20000	0.528%	*0.775%*
40000	0.389%	*0.631%*
60000	0.322%	*0.561%*
80000	0.282%	*0.517%*
100000	0.255%	*0.486%*
150000	0.215%	*0.439%*
200000	0.192%	*0.410%*

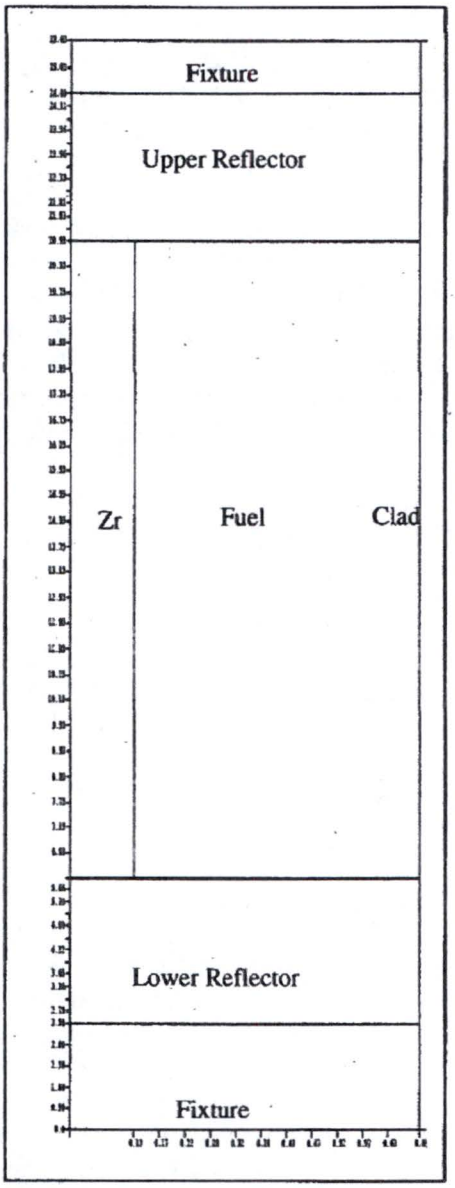

(R-axis and z-axis not to same scale)

Figure 13-1 Outline of AFFRI TAC2D LOCA Model Geometry

The radial axis - r_{max}=0.7065 in. (1.795 cm) is scaled differently than the axial axis - z_{max}=23.70 in. (60.20 cm). The fuel rod axial and radial lengths give a rod aspect ratio of 33.6:1. Using the same scale for both axes would give a long narrow figure with details lost. Thus, the un-equal axes scaling is used.

Thermal properties of the rod components and radial and axial power profiles are taken from the steady state thermal analysis performed in Section 4.7. Thermal contact resistances are incorporated between component contacts in the axial direction. The thermal conductance specified for these contacts is 30 BTU/hr-ft^2-°F (51.92 W/m^2-K). A radial conductance of 400 BTU/hr-ft^2-°F (692 W/m^2-K) is specified for the radial contact between the fuel and the clad. A radial gap of 0.1 in. (2.54 mm) is placed between the graphite reflectors and the clad. Thermal radiation between these two components is included in the model. The end fixtures are welded to the clad, so no significant thermal resistance occurs radially between these two components. The 0.5 in. (1.27 cm) high void between the top graphite reflector and the top fixture is modeled with natural convection and radiation from its surfaces. Neither conduction nor radiation is assumed to occur from the ends of the rod to the grid plates or other components of the core. The model also does not include thermal radiation radially between the hot rod and other cooler rods in the core.

Equations are added to the TAC2D model to compute the natural convection air flow through the hot rod flow channel. The following two equations govern the air up-flow from the pool below the core to the pool above the core:

$$P_{Pb}-P_{Pt}=[K_{in}^{'}+1-(\frac{A_c}{A_{Pb}})^2]\frac{m^2}{2\rho A_c^{\,2}}+\int_0^{L_{hot}}\frac{4f}{d_h}\frac{m^2}{2\rho A_c^{\,2}}dz+(\frac{1}{\rho_b}-\frac{1}{\rho_t})\frac{m^2}{A_c^{\,2}}$$
$$+[K_{out}^{'}-1+(\frac{A_c}{A_{Pb}})^2]\frac{m^2}{2\rho A_c^{\,2}}+\bar{\rho}_{hot}gL_{hot} \qquad (3)$$

$$P_{Pb}-P_{Pt}=\rho_{cold}gL_{cold} \qquad (3a)$$

The first equation, which is the momentum equation applied to the air up-flow, is adapted from Equation 2-26a of Shah, 1978 (Reference 13-5). The first term on the right-hand side represents the inlet pressure loss and the acceleration of air flow from the bottom of the core into the hot rod flow channel. The density in this term is evaluated at the core inlet temperature. The second term on the right is the wall friction loss along the rod exterior. This term is integrated numerically from the bottom of the rod to the top of the rod. The third term represents the pressure decrease in the flow direction due to the flow acceleration from a cold inlet to a hot outlet. The densities in this term are evaluated at the core inlet temperature and the core outlet temperature, respectively. The fourth term is the flow exit loss from the hot channel to the core outlet. The last term is the density head of the hot channel. Equation 3a represents the static head of the cooler down-flow air outside of and parallel to the core.

The equations for the flow lengths in these two equations are:

$$L_{rod} = L_{bot\_fixture} + L_{bot\_refl} + L_{fuel} + L_{top\_refl} + L_{void} + L_{top\_fixture} \quad (4)$$

$$L_{hot} = L_{rod} + L_{plume}, \qquad L_{cold} = L_{hot} \quad (4a)$$

L_{rod} is the length of the fuel element over that portion where the diameter is the constant fuel element diameter. L_{rod} equals the lengths of the lower fixture (constant diameter portion), lower reflector, fuel region, upper reflector, void length, and upper fixture (constant diameter portion). L_{hot} equals this rod length plus the assigned plume length. The assigned plume length equals ten channel hydraulic diameters (a typical length where the core of a hot plume mixes completely with cooler surroundings and where this core temperature begins to decrease).

The core dimensions and K losses used for equations 4 and 4a, and applied to the AFRRI reactor are:

d_{rod} – fuel element dia. – (b)(7)(F)

L_f – heated fuel length – (b)(7)(F)

$L_{bot\_fixture}$ – bottom fixture length – 0.5 in. (1.27 cm)

$L_{reflector}$ – lower and upper reflector lengths – 3.42 in. (8.687 cm)

L_{void} – length (height) – 0.5 in. (1.27 cm)

$L_{top\_fixture}$ – top fixture length – 0.86 in. (2.1844 cm)

L_{rod} – length – 23.70 in. (60.20 cm)

A_c – flow area in fuel region for one fuel element – (b)(7)(F)

A_p – flow area outside the core, assumed large relative to A_c

d_h – flow hydraulic dia. – 0.6302 in. (1.601 cm)

L_{plume} – plume length, 10 d_h's, adds to the hot density head – 6.302 in. (16.01 cm)

$K_{loss\ inlet}$ – 1.30; $K_{loss\ outlet}$ – 0.3. K's are referenced to the fuel section flow area, A_c.

Other input for the LOCA analysis:

- Reactor operating power before shutdown – 1.0 MW
- Core temperature at beginning of decay heat – 48°C (118.4°F)
- Core inlet air temperature – 27°C (80.6°F)

This input is based on the following assumptions: reactor is operating at nominal steady state power, pool return water is at its maximum allowable temperature of 48°C and this water cools the core to the same temperature, and room air temperature is at 27°C (this is the core air inlet temperature).

Figure 13-2 shows the rod locations for a grouping of the single A-ring rod, two B-ring rods, and three C-ring rods.

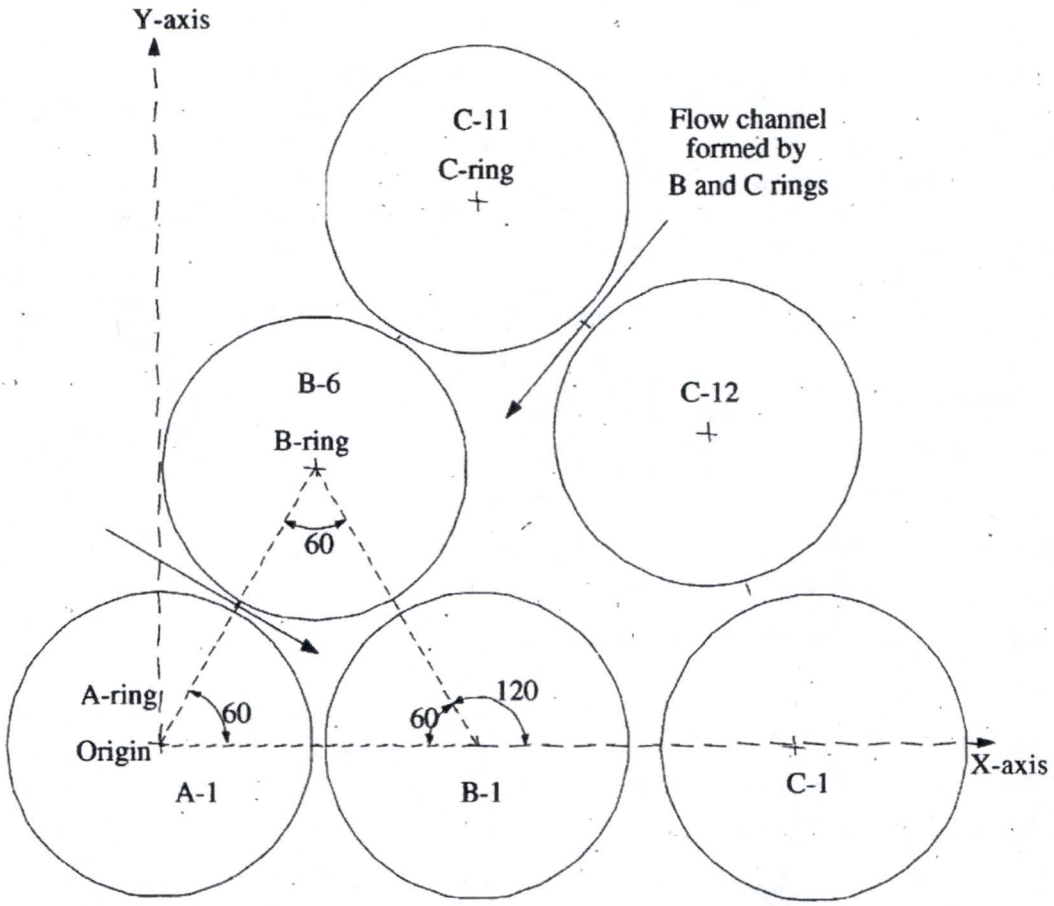

Figure 13-2 AFFRI Rod Layout for a Symmetric Portion of the A, B and C Rings

This grouping of six rods occurs six times within 360°. Thus, one such group would contain the hot rod. We will assume rod B-1 is the hot rod. (The true hot rod may be in one of the other six rod groups, and the following logic still applies.) In TRIGA thermal analyses, an independent flow area is usually defined as the location of the minimum gap between adjacent rods. It is argued that little cross-flow occurs across these minimum gaps, and the included flow area may be considered independent. One such area is the small tri-cusp flow area bounded by rods A-1, B-1 and B-6. Rod B-1 (each rod also) shares 1/3 of the total tri-cusp area. A second larger flow area is defined within the five rods B-1, B-6, C-11, C-12, and C-1. Rod B-1 shares 0.2222 of

(b)(7)(F)

minute delay curve is the more realistic result, since the delay time represents the time for the pool to drain. Either curve shows there is considerable margin between these peak temperatures and the maximum allowable fuel temperature of 950°C (1742°F).

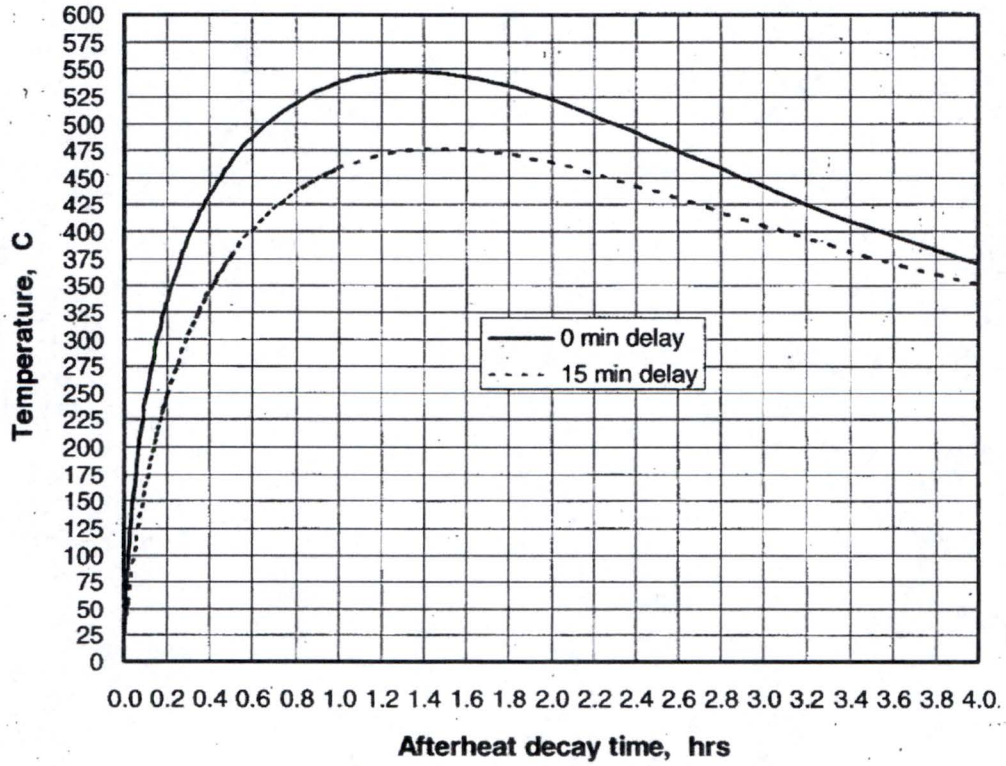

Reactor Operation for 72 Hours/Week for 40 Years

Figure 13-3 Maximum Fuel Temperature versus Afterheat Decay Time

13.2.1.4 LOCA Radiation Exposure

If the water shield is lost, the possible exposure to AFRRI personnel or the general public would be due to direct or scattered gamma radiation from the exposed reactor fuel inside the reactor tank.

To calculate the dose rate after the LOCA, an MCNP model was made and the gamma source terms on several operation times and the times after shutdown were evaluated for the calculations.

The following assumptions have been made for the irradiated fuel in the analysis of postulated gamma doses within the reactor room and outside the AFRRI facility:

1. Power level = 1 MW(t) (steady-state operation)
2. Volume of fuel elements = (b)(7)(F) cm^3
3. Distance from top of core to reactor tank top = 505 cm
4. Distance from reactor room floor to ceiling = 550 cm
5. Reactor tank diameter = 366 cm
6. Ceiling thickness = 10 cm of ordinary concrete
7. Density of fuel element = 7.58 gm/cm^3

Using the above assumptions, a three dimensional MCNP model was made for the dose rate calculations. The fuel elements were modeled as a right cylinder with radius of 16.55 cm and height of 38.1 cm.

The gamma source term in the fuel elements depends on how long the reactor was operating prior to shutdown and the time after shutdown.

The decay heat from the fission products after the reactor has been shutdown can be expressed by (Ref 13-7):

$$\frac{P}{P_0} \approx 6.5 \times 10^{-2}[(\tau - T_0)^{-0.2} - \tau^{-0.2}]$$

Where: P = the decay heat (or power) rate at time τ (second),
P_0 = the core operating thermal power,
$\tau - T_0$ = the time after shutdown (second)

The decay heat (power) ratios for various operation times and for times after shutdown are calculated by using the above equation, and are listed in Table 13-2.

Table 13-2 The decay heat (power) ratios for various operation time and the time after shutdown.

Operation Time	Decay Heat Ratio (P/Po) for Time After Shutdown				
	1 sec	15 min	30 min	1 hr	1 day
7 days	6.05E-02	1.21E-02	9.98E-03	8.11E-03	2.28E-03
14 days	6.11E-02	1.27E-02	1.06E-02	8.69E-03	2.80E-03
30 days	6.16E-02	1.33E-02	1.11E-02	9.25E-03	3.33E-03
100 days	6.23E-02	1.40E-02	1.19E-02	9.97E-03	4.03E-03

The decay heat is from the both of gamma and beta radiations in the fission products. However, because the beta radiation cannot penetrate the cladding materials, only the gamma radiations were considered in the dose calculation. The power ratios in Table 13-3 are from the gamma radiations only, and they were derived by multiplying the Table 13-2 values by a factor of 0.462. The gamma contribution to the decay heat was estimated by 6 MeV (gamma energy released from fission products per each fission) divided by 13 MeV (gamma plus beta energy released from fission products per each fission).

Table 13-3 The gamma decay heat (power) ratios for various operation times and the time after shut down.

Operation Time	Gamma Decay Heat Ratio (P/Po) for Time After Shutdown				
	1 sec	15 min	30 min	1 hr	1 day
7 days	2.79E-02	5.60E-03	4.61E-03	3.74E-03	1.05E-03
14 days	2.82E-02	5.87E-03	4.88E-03	4.01E-03	1.29E-03
30 days	2.84E-02	6.13E-03	5.14E-03	4.27E-03	1.53E-03
100 days	2.88E-02	6.47E-03	5.47E-03	4.60E-03	1.86E-03

To make a conservative approach to the gamma dose rate calculation, the gamma energy was assumed as 1 MeV. The schematic of the R-Z MCNP model is shown in Figure 13-4A, and the calculated MCNP result is shown in Figure 13-4B.

The result shown in the figure is per gamma source (1 MeV/sec), the dose rate is in rem/hr, and these values were obtained with an option in the code that uses the photon flux-to-dose rate conversion factors from ANSI/ANS 6.1.1, 1991.

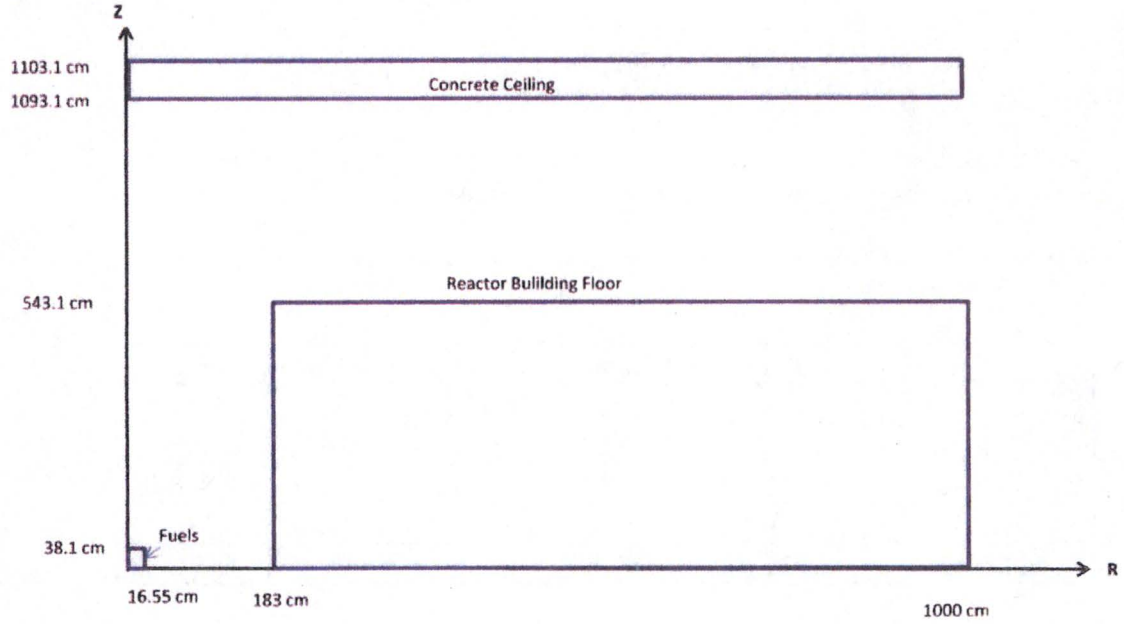

Figure 13-4A The schematic of the R-Z MCNP model

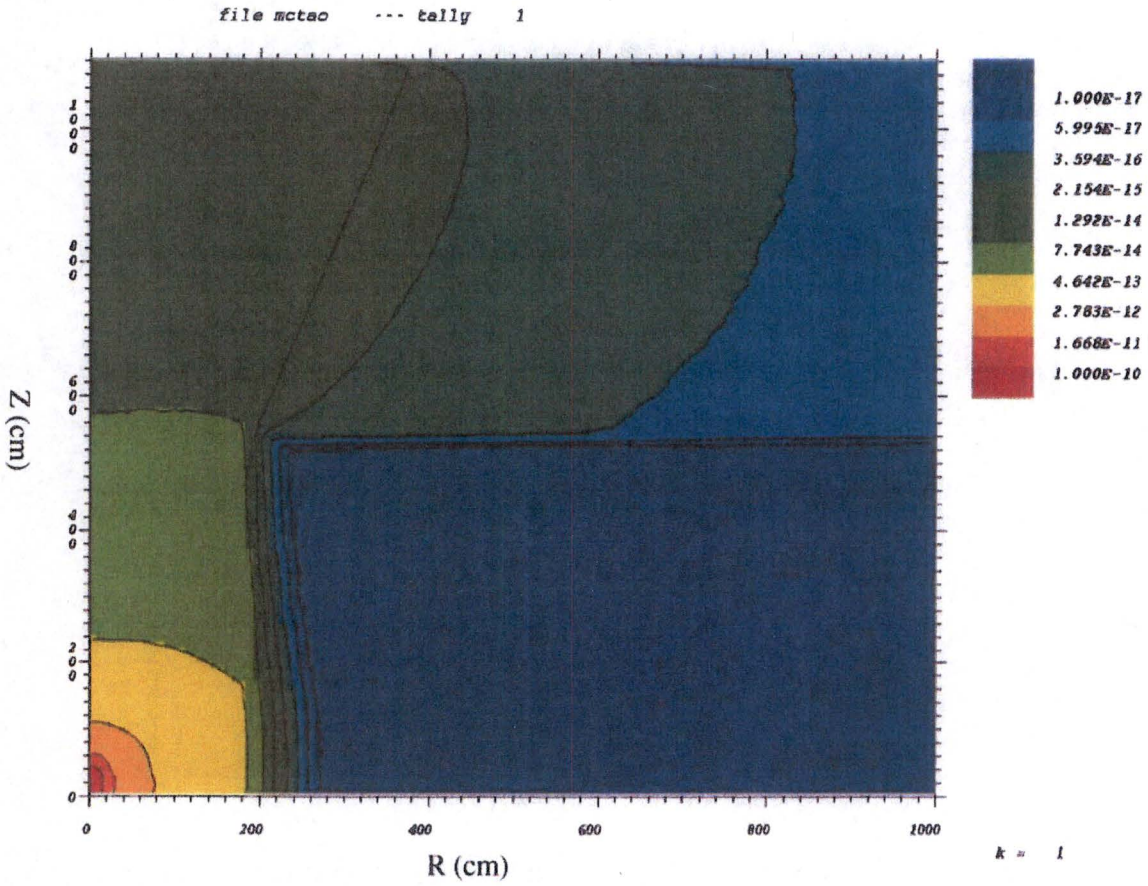

Figure 13-4B The calculated R-Z dose rates (rem/hr) per 1 MeV gamma.

The gamma source terms for various operation times and the time after shutdown are listed in Table 13-4. The calculated dose rate can be obtained by multiplying the appropriate gamma source to the MCNP results with the per gamma source as shown in Figure 13-4B.

Table 13-4 The gamma source (MeV/sec)

Operation Time	Gamma Source (MeV/sec) for Time After Shutdown				
	1 sec	15 min	30 min	1 hr	1 day
(b)(7)(F)					

The axial dose rates for various times after shutdown at the center of the core (R = 0) for 100 days of operation are shown in Figure 13-5. The calculated time dependent surface dose rates (R = 0 to 16.55 cm) for several axial locations are listed in Table 13-5. The dose rate at the top surface of the core varies from 1.83×10^7 rem/hr to 1.19×10^6 rem/hr as the shutdown time changes from 1 second to 1 day.

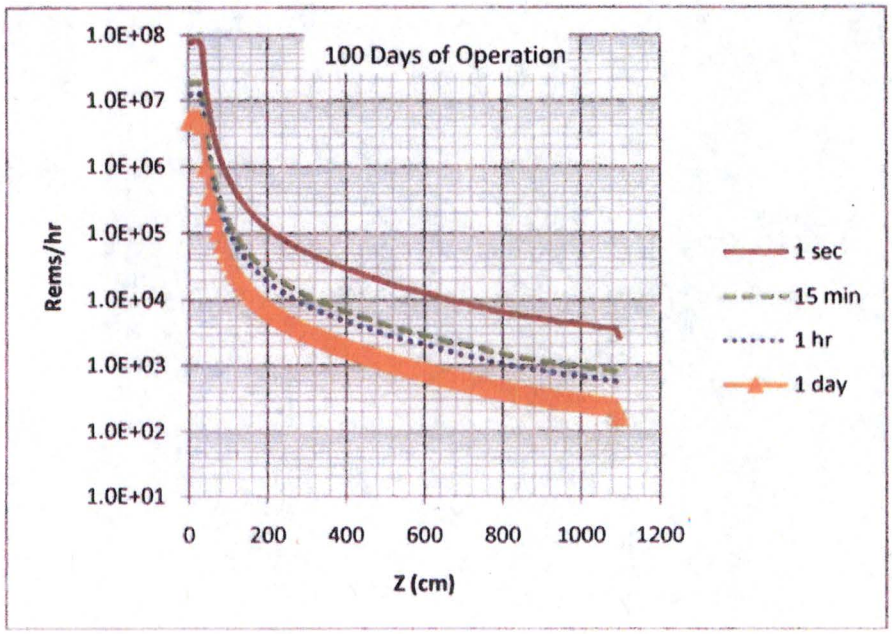

Figure 13-5 The axial dose rates (rem/hr) at R = 0 for 100 days of operation.

Table 13-5 The calculated surface dose rates for several locations with 100 days of operation. (The surface dose rates are averaged over R = 0 to R = 16.55 cm)

Location	Z (cm)	Dose Rate (rem/hr) Time after Shutdown				
		1 sec	15 min	30 min	1 hr	1 day
Top of the Core	38.1	1.83E+07	4.12E+06	3.48E+06	2.93E+06	1.19E+06
Reactor Bldg. Floor	543.1	1.59E+04	3.57E+03	3.02E+03	2.54E+03	1.03E+03
Ceiling	1093.1	3.54E+03	7.95E+02	6.72E+02	5.66E+02	2.29E+02
Top of the Roof	1103.1	1.39E+03	3.11E+02	2.63E+02	2.22E+02	8.97E+01

The variation of the surface dose rates at the roof top is shown in Table 13-7. When the radius is greater than 400 cm the surface dose rate decreases significantly. This is mostly because the direct radiation from the fuel near the bottom of the pool cannot reach the pool surface.

Table 13-7 The surface dose rate (rem/hr) at the roof top (Z = 1103.1 cm)

R (cm)	Dose Rate (rem/hr) Time After Shutdown				
	1 sec	15 min	30 min	1 hr	1 day
0 to 16.55	1.39E+03	3.11E+02	2.63E+02	2.22E+02	8.97E+01
16.55 to 183	1.34E+03	3.01E+02	2.55E+02	2.14E+02	8.67E+01
183 to 400	1.10E+03	2.48E+02	2.10E+02	1.77E+02	7.14E+01
400 to 600	4.29E+01	9.65E+00	8.16E+00	6.87E+00	2.78E+00
600 to 800	1.27E+01	2.85E+00	2.41E+00	2.03E+00	8.20E-01
800 to 1000	4.86E+00	1.09E+00	9.23E-01	7.77E-01	3.14E-01

13.2.2 Radioactive Contamination of Reactor Shielding Water

Contaminant material susceptible to neutron irradiation in the shield water is maintained at low concentrations by the water purification system and an in-line set of particulate filters which remove particulates of 5 microns or larger. The consequences associated with a failure of the fuel element cladding and subsequent fission product contamination of the water have been calculated and studied experimentally, as described in Section 13.2.3. The results show that in the improbable event of fuel element cladding failure, the water can be decontaminated by the resins of the purification system. Manufacturing inspection and quality controls assure that the possibility of cladding failure is minimal.

Experiments conducted over a period of 11 years by General Atomics on 8.5 wt% U-ZrH (8.5 weight percent uranium) fuel elements under various conditions have shown that a small fraction of fission products are released from U-ZrH fuel into the gap between the fuel and cladding. This release fraction varies from less than 1.5×10^{-5} for an irradiation temperature of 350°C to a theoretical maximum of 1.0×10^{-2} at 800°C.

Three mechanisms (recoil, diffusion, and dissolution) have been shown to be involved in fission product migration. The first mechanism is the fission fragment recoil into the gap between the fuel and cladding. This effect predominates at temperatures up to approximately 400°C. In this range, the recoil release rate is dependent on the fuel surface-to-volume ratio but is independent of temperature. This is the most important mechanism in this system and is considered in the calculations dealing with fission product release following fuel element cladding failure. At temperatures above approximately 400°C, the diffusion-like process predominates. The amount released is dependent on the fuel temperature, the fuel surface-to-volume ratio, the length of time of irradiation, and the isotope half-life. This mechanism is of little significance to the fission product release fraction considered in this system. The U-ZrH is relatively chemically inactive in water, steam, and air at temperatures up to about 850°C. Massive zirconium hydride has been

heated in air for extended periods of time at temperatures up to 600°C with negligible loss of hydrogen. This negligible loss of hydrogen is due to oxide film formation which inhibits hydrogen loss.

13.2.3 Fuel Element Cladding Failure

13.2.3.1 Summary of Previous Experience

Following the original development of the TRIGA reactor, General Atomics maintained a program of research and development that led to improvement in the fuel element design so that TRIGA reactors could be operated in both steady-state and pulsing modes without undue concern regarding fuel integrity.

Extensive operational testing of TRIGA fuel elements was conducted by General Atomics in the Torrey Pines TRIGA and the prototype TRIGA Mark-F beginning in the early 1960s. Experiments on fuel with 8.5 wt% uranium were conducted over a period of 11 years under a variety of conditions. These experiments included:

- 1960 - The measurement of the quantity of a single fission product isotope released from a full-size TRIGA fuel element during irradiation.
- 1966 - The measurement of the fractional release of several isotopes from small specimens of TRIGA fuel material during and after irradiation at temperatures ranging from approximately 25°C to 1100°C.
- 1971 - The measurement of the quantities of several fission product isotopes released from a full-size TRIGA fuel element during irradiation in a duplication of the 1960 experiment.

In addition, quench tests were performed on TRIGA low-enriched uranium (LEU) fuel samples for temperatures ranging from 800°C to 1200°C. The subsequent fuel samples quenched from 800°C, 1000°C, 1100°C, and 1200°C showed remarkably benign response to the test conditions.

In the course of developing a reactor for pulse operation, General Atomics experienced three fuel element cladding failures in their Torrey Pines TRIGA reactor. These cladding failures were of two types:

- Two aluminum cladding failures resulted from mechanical ratcheting of the cladding material induced by thermal cycling.
- A cladding failure associated with an aluminum-clad element instrumented with internal thermocouples.

In the original TRIGA fuel element design, aluminum cladding was used and mechanical ratcheting occurred during pulse operations. Modification of the standard TRIGA fuel element design by replacing aluminum with stainless steel as the cladding material during the mid-1960s eliminated this cause of failure. The present stainless steel cladding has greater durability than the original aluminum which experienced the metal cladding failures. The other cladding failure

involving an instrumented element was apparently the result of either internal pressure buildup or water seepage.

The consequences of these cladding failures at General Atomics were all minor and in the worst case experience (which involved the cladding failure of an element instrumented with internal thermocouples and which had experienced a steady-state burnup of ~22 MW-hrs and a pulse burnup of ~3 MW-hrs involving pulses as high as $4.00) may be summarized as follows:

- The activity in the reactor water reached a maximum of 0.2 $\mu Ci/cm^3$. It decayed very rapidly and was measured 24 hours after the cladding failure to be 5×10^{-5} $\mu Ci/cm^3$, a 4,000-fold reduction.
- The activity in the air of the reactor room reached approximately 10 times the occupational derived air concentration (DAC) for fission products and then decayed rapidly. The faulty fuel element was removed and experiments were resumed 2 hours after the activity release. The maximum integrated dose to operating personnel resulting from this release was 1 mrem.
- The noble gases were not collected on the air monitor filters used, but it may be inferred from the nature of the particulates collected that only noble gas fission products escaped from the TRIGA pool in significant proportions when the fuel cladding failed.

It was concluded from these General Atomics experiments and actual cladding failure experiences that a cladding failure, or even the simultaneous failure of the cladding of several fuel elements, would not constitute an undue risk to the health and safety of the operating personnel or the general public.

13.2.3.2 Calculation of Maximum Fission Product Release After a Fuel Element Cladding Failure

Calculations and a related experiment have been made to determine the maximum concentration of fission products that might be present in the reactor room air following the Design Basis Accident of a fuel element cladding failure.

The calculations are based on the fact that as the reactor operates, the fission products will build in the uranium-zirconium fuel mixture until an equilibrium concentration is reached for each nuclide. The resulting equilibrium nuclide concentration of fission products depends upon the total energy release in the reactor, the decay process for each nuclide, and the yield of the species from fission. Only the kryptons, xenons and iodines will migrate into the gap between the fuel material and fuel element cladding.

To determine the various inventories of fission products produced in the core, data were used from Meek, 1968 (Reference 13-8) for infinite steady-state power operation at 1 MW(t). The resultant full power steady-state inventories for the kryptons, xenons, and iodines were calculated and are shown in Table 13-8.

Table 13-8 Gaseous Fission Product Inventory for 1 MW Steady-State Operation

Isotope	Half-Life	Fission Yield (%)	Saturation Activity (Ci)	Gamma Source Strength (MeV/sec)
Krypton (Kr)				
83	(b)(7)(F)	(b)(7)(F)		
85m				
85				
87				
88				
89				
Total				
Xenon (Xe)				
131m				
133m				
133				
135m				
135				
137				
138				
Total				
Iodine (I)				
131				
132				
133				
134				
135				
Total				
Gaseous Total				

The associated fission product inventory for an assumed 40 MW-sec maximum pulse was also calculated from Meek, 1968 (Reference 13-8) with the buildup and decay of activities from Bolles, 1956 (Reference 13-9) considering only prompt fission events in the pulse. The resultant 40 MW-sec pulse inventories for kryptons, xenons, and iodines are shown in Table 13-9.

Table 13-9 Gaseous Fission Product Inventory for 40 MW-sec Pulse Operation

Isotope	Half-Life	Fission Yield (%)	One-Minute Decay Activity (Ci)	Gamma Source Strength (MeV/sec)
Krypton (Kr)				
(b)(7)(F)				
Total		(b)(7)(F)		
Xenon (Xe)				
(b)(7)(F)				
Total		(b)(7)(F)		
Iodine (I)				
(b)(7)(F)				
Total		(b)(7)(F)		
Gaseous Total		(b)(7)(F)		

For those isotopes with relatively long half-lives, low fission yields, or complex decay chains, the activity present from pulse operation will not be significant. Such isotopes include Kr^{83m}, Kr^{85}, Xe^{131m}, Xe^{133}, Xe^{133m}, and I^{131}.

These inventories are utilized in the calculation of radiological consequences associated with the various fuel element cladding failures which may result during the operation of the AFRRI-TRIGA reactor. The gamma source strengths were derived using gamma energy decay data from Lederer, 1978 (Reference 13-10) and are shown in Tables 13-8 and 13-9.

In order to determine the actual percentage of fission product gases that escape from the fuel material and collect in the gap between the cladding and the fuel material, experiments were conducted in the TRIGA reactor at General Atomics. A fuel element was fabricated with a sealed tube that vented the gap to a charcoal-filled cold trap at the surface of the reactor tank. All of the fission product gases that accumulated in the gap were collected in the liquid-air-cooled charcoal trap by purging the system with helium, and the trap was analyzed. This measured amount of radioactive noble gases enabled the determination of the fraction of the fission products that diffused through the uranium-zirconium hydride material into the gap.

Although the measured amount of radioactive noble gases for the operating conditions in the AFRRI reactor fuel would indicate a gap activity percentage of less than 0.01 percent, the theoretical limit of 0.1 percent gap activity for fission product gases of noble gases and iodines, as stated in GA, 1980 (Reference 13-1) will be used in the consequence analysis for this Design Basis Accident.

As shown in Table 13-8, the total quantity of all gaseous fission products in a TRIGA core for 1 MW operation at equilibrium is (b)(7)(F) curies. For the purposes of this calculation, it is conservatively assumed that the fractions of the iodine, krypton, and xenon isotopes produced that collect in the gap between the fuel material and fuel cladding and, therefore, available for release are 0.1 percent, corresponding to a fuel temperature of 600°C. Thus, the total core activity in the gap is calculated to be [redacted] curies. The maximum amount of fission products that could be released in the event of a cladding failure of a single average fuel element for an average 85 fuel element AFRRI-TRIGA core is less than [redacted] curies during steady-state operation. As shown in Table 13-9, the total quantity of all gaseous fission products from a 40 MW-sec pulse operation is (b)(7)(F) curies in the core with a gap activity of [redacted] curies. The additional release in the event of a cladding failure in an average fuel element is less than [redacted] curies. The total release from a cladding failure event is approximately [redacted] curies from an average fuel element during pulse operation following steady-state operation.

The volume of water in the TRIGA reactor tank is approximately 5.7×10^7 cm^3 and the volume of air in the reactor room is approximately 9.2×10^8 cm^3. For the purpose of calculation, it is assumed that all of the gaseous fission products in the gap are available for release. As concluded from measurements of the worst cladding failure experienced, only noble gas fission products would be expected to escape from the TRIGA pool when the fuel cladding fails. Due to the low pressure in the gap and the small gap size in a TRIGA fuel element, any iodine released from the fuel element due to a cladding failure is expected to be completely dissolved in the pool water. However, for calculation purposes, it is conservatively assumed that as much as 0.2 percent of the iodine released from the fuel element due to a cladding failure and all of the kryptons and xenons could be released into the reactor room atmosphere. The release assumptions are used to determine the radiological consequences due to the Design Basis Accident of a fuel element cladding failure. Of the [redacted] curies that could be released from the gap in the cladding failure of an average fuel element, less than [redacted] curies would be radioiodine, while the remaining [redacted] curies would be krypton and xenon. Therefore, the concentration in the water would be less than [redacted] µCi/cm^3, while the air concentration would be less than [redacted] µCi/cm^3.

Since krypton and xenon are inert gases, the exposure due to their presence in air is from submersion exposure from a spherical source. The gamma source strengths for the kryptons, xenons, and iodines are given in Table 13-8 for steady-state operation and Table 13-9 for pulse operation. As previously determined, the volume of the reactor room is approximately 9.2×10^8 cm^3, which is equivalent to a sphere with a radius of 603 cm. The gamma source strength from kryptons and xenons for steady-state operation is calculated as (b)(7)(F) MeV/sec, while for pulse operation it is calculated as (b)(7)(F) MeV/sec, or a total of (b)(7)(F) MeV/sec. Using the gap activity as 0.1 percent and an 85 fuel element core, the cladding failure of an average fuel element will release (b)(7)(F) MeV/sec of kryptons and xenons into the reactor room volume.
(b)(7)(F) The air concentration of — $\mu Ci/cm^3$ previously calculated is equivalent to a gamma volume source strength of (b)(7)(F) MeV/cm^3-sec.

For the noble gas mixture, the linear attenuation for air is 9.7×10^{-5} cm^{-1} and the flux-to-dose conversion factor is 5×10^5 MeV/cm^2-sec per rads/hr assuming a 0.7 MeV gamma photon. Substituting these values into the appropriate equation results in a dose rate in the reactor room from the calculated noble gas concentration of about 0.2 rads/hr. Within an hour, the dose rate in the reactor room will be reduced to less than 0.1 rads/hr.

Based upon these conservative calculations for a fuel element cladding failure during pulse operation following steady-state operation, a person could remain in the reactor room for more than 50 hours before exceeding the allowable yearly occupational dose limit of 5 rem (TEDE).

Standard operational procedures require prompt evacuation of personnel following an indication of excessive airborne radioactivity in the reactor room. Reentry to the reactor room would be determined by the Reactor Facility Director when the airborne concentration was safe for normal operations to resume.

13.2.3.3 Calculation of Offsite Consequences After a Fuel Element Cladding Failure

The diffusion factor (χ/Q) and finite cloud correction factors are dependent upon the distance from the source and are presented in Table 13-10.

Table 13-10 Diffusion Factor and Finite Cloud Correction Factor

Distance (m)	χ/Q (sec/m^3)	Finite Cloud Correction Factor
25	1.0 E-1	1.5 E-2
50	2.7 E-2	2.7 E-2
75	1.2 E-2	4.2 E-2
100	7.5 E-3	5.5 E-2
150	3.7 E-3	8.0 E-2
200	2.2 E-3	1.0 E-1

These parameters are based upon a Pasquill type F stability condition with a 1 m/sec wind speed and a cross sectional area for the AFRRI facility of 450 m^2. The methodology in NRC, 1983

(Reference 13-11), was used to determine the diffusion factor. The methodology described in Slade, 1968 (Reference 13-12), for defining the ratio of gamma dose from a finite cloud to an infinite cloud with the same centerline concentration was used to determine the finite cloud correction factor. Table 13-11 presents the source terms of radioactivity and thyroid and gamma source strengths postulated to be released to the atmosphere from the AFRRI reactor room.

Table 13-11 Gaseous Fission Products Released to Atmosphere Following Fuel Element Clad Failure Accident

Isotope	Activity (Ci)	Gamma Source Strength (MeV/sec)	Thyroid Source Strength (rads)
Krypton	(b)(7)(F)		--
Xenon			--
Iodine			(b)(7)(F)
TOTAL			

To calculate the whole body gamma dose to an individual outside the AFRRI facility, the following equation was utilized:

$$D\gamma = 0.25\,(E\gamma)\,(Q)\,(\chi/Q)\,(F) \qquad (9)$$

Where:
- $D\gamma$ = integrated whole body gamma dose (rem)
- $E\gamma$ = gamma energy released per disintegration (MeV/dis)
- Q = total activity released (Ci)
- χ/Q = diffusion coefficient (sec/m^3)
- F = ratio of gamma dose from finite cloud to infinite cloud

To calculate the thyroid dose to an individual outside the AFRRI facility, the following equation was utilized:

$$D_{th} = (BR)\,(\chi/Q)\,(S_{th}) \qquad (10)$$

Where:
- D_{th} = integrated thyroid dose (rem)
- BR = breathing rate = 3.47×10^{-4} m^3/sec
- χ/Q = diffusion coefficient (sec/m^3)
- S_{th} = (DCF) (Q), iodine inhalation source term (rem)
- DCF = dose conversion factor (rem/Ci)
- Q = iodine activity released (Ci).

The conservative assumption is made that the radioactive gases released in the AFRRI reactor room will be released directly to the atmosphere without significant holdup within the facility.

The current design of the AFRRI reactor room would cause isolation of the reactor room by automatic closure of the ventilation pathway to the AFRRI stack and would prevent excessive leakage to other parts of the AFRRI facility past the access doors that are sealed with compressible gaskets.

The calculated whole body dose is insignificant at all distances downwind from the AFRRI facility. The maximum calculated whole body dose is less than 2 mrem or a factor of 500 below the Protective Action Guide (PAG) whole body dose of 1 rem, below which no protective action is recommended. The maximum calculated on-site thyroid dose of 57 mrem is nearly a factor of 90 below the PAG thyroid committed dose equivalent of 5 rem, below which no protective action is recommended. The calculated thyroid dose for individuals beyond the boundary of the NNMC site would be well below 1 mrem.

13.2.4 Fuel Element Drop Accident

A Design Basis Accident for the AFRRI reactor is postulated to be the occurrence of a cladding failure of a fuel element after a 2-week period where the saturated fission product inventory of a 1 MW steady-state operation (100 hours to reach saturated fission product inventory) has been allowed to decay after being taken out of the operating core and placed in storage. The cladding failure is postulated to occur when the fuel element is withdrawn from the reactor pool. When the fuel element is exposed to air, a cladding failure could occur coincidentally, or due to a drop of the fuel element. The probability of such an accident is considered to be extremely remote. The probability of cladding failure has been further reduced under the postulated accident conditions by the substitution of stainless steel cladding for the former aluminum cladding on the fuel elements. The fission products released from the gap will depend upon the temperature of the fuel following 2 weeks decay. This temperature is expected to be less than 50°C. The temperature needed to volatilize iodine (183°C) is, therefore, not reached and gaseous iodine should not be released. The kryptons and xenons will be in the gaseous state and would be released (100 percent). Although iodine will not be volatile under the assumed accident conditions, a release of 1 percent of the gap activity has been assumed for calculational purposes. The data in Table 13-10 as well as equations (9) and (10) were used in the evaluation of this accident to calculate the whole body and thyroid doses to individuals downwind from the AFRRI facility.

Table 13-12 presents the source terms of radioactivity and thyroid and gamma source strengths in the total core for 1 MW steady-state operation after 2 weeks of decay.

Table 13-12 Gaseous Fission Product Inventory for 1 MW Steady State Operation with 2-Week Decay

Isotope	Activity (Ci)	Gamma Source Strength (MeV/sec)	Thyroid Source Strength (rad)
Krypton (Kr)			
(b)(7)(F)			--
Xenon (Xe)			
(b)(7)(F)			--
			--
			--
Total	(b)(7)(F)		--
Iodine (I)			
(b)(7)(F)			
Total	(b)(7)(F)		
Gaseous Total			

These values are to be reduced to 0.1 percent for the gap activity and for the 85 fuel element core to determine the amount of fission products that might be released in an average fuel element drop accident resulting in cladding failure. The total release is less than [redacted] curies with a (b)(7)(F) gamma source strength of (b)(7)(F) MeV/sec. The iodine release fraction is assumed to be 1 percent for a thyroid source strength of 1.3×10^3 rads. The same conservative assumption made for the fuel clad failure accident in Section 13.2.3.3 regarding the prompt release of radioactive material to the atmosphere has been made for this Design Basis Accident.

The calculated whole body dose is insignificant at all distances downwind from the AFRRI facility. The maximum calculated thyroid dose of 45 mrem is more than a factor of 100 below the PAG thyroid committed dose equivalent of 5 rem, below which no protective action is recommended. The calculated thyroid dose for individuals beyond the boundary of the NNMC site within which the AFRRI facility is located would be significantly less than 1 mrem.

References

13-1 General Atomics, 1980, "The U-ZrHx Alloy: Its Properties and Use in TRIGA Fuel", GA Report E-117-833, February 1980.

13-2 Simnad, M. T., et al, 1976, "Fuel Elements for Pulsed TRIGA Research Reactors", Nuclear Technology 28, no. 31, pp. 31-56, January 1976.

13-3 American Nuclear Society, 2005, "Decay Heat Power in Light Water Reactors", ANSI/ANS-5.1-2005.

13-4 General Atomics, 1976, "TAC2D: A General Purpose Two-Dimensional Heat Transfer Computer Code User's Manual", GA-A14032, July 1976.

13-5 Shah, R. K. and A. L. London, 1978, "Laminar Flow Forced Convection in Ducts", Academic Press, 1978.

13-6 NRC, 1987, "Safety Evaluation Report on High-Uranium Content, Low Enriched Uranium-Zirconium Hydride Fuels for TRIGA Reactors", Docket No. 50-163, NUREG-1282, U.S. Nuclear Regulatory Commission, August 1987.

13-7 Glasstone and Sesonske, (1981), "Nuclear Reactor Engineering," Equation (2.65), P. 122, 3rd Edition, Van Nostrand Reinhold Company, 1981.

13-8 Meek, M. E., and B. F. Rider, 1968, "Summary of Fission Yields for U-235, U-238, Pu-239, Pu-241 at Thermal, Fission Spectrum, and 14 MeV Neutron Energies," APED-5398-A (Revised), October 1, 1968.

13-9 Bolles, R. C., and N. E. Ballou, 1956, "Calculated Activities and Abundances of U-235 Fission Products," USNRDL-456, August 30, 1956.

13-10 Lederer, C. M., and Virginia Shirley, 1978, "Table of Isotopes, 7th edition, New York: John Wiley & Sons, Inc., 1978.

13-11 NRC, 1983, "Atmospheric Dispersion Models for Potential Accident Consequence Assessments at Nuclear Power Plants," Regulatory Guide 1.145, Revision 1 (w/correction), February 1983.

13-12 Slade, David H., ed., 1968, "Meteorology and Atomic Energy – 1968," Air Resources Environmental Laboratories, Environmental Science Services Administration, U.S. Dept. of Commerce, July 1968.